ELSEVIER

J. Non-Newtonian Fluid Mech. 144 (2007) 122–139

Journal of Non-Newtonian Fluid Mechanics

www.elsevier.com/locate/jnnfm

A network scission model for wormlike micellar solutions I. Model formulation and viscometric flow predictions

Paula A. Vasquez [a,*], Gareth H. McKinley [b], L. Pamela Cook [a]

[a] *Department of Mathematical Sciences, University of Delaware, Newark, DE 19716, USA*
[b] *Department of Mechanical Engineering, Massachusetts Institute of Technology, Cambridge, MA 02139, USA*

Received 6 December 2006; received in revised form 19 March 2007; accepted 20 March 2007

Abstract

In this paper a network model for wormlike micellar solutions is presented which incorporates scission and reforming of the chains, based on a discrete version of Cates' 'living polymer' theory. Specifically we consider two elastically active Hookean species: long chains which can break to form two short chains, which can themselves recombine to form a long chain. The chains undergo rupture at a rate dependent on the local elongation and deformation rate. This two species model, developed ultimately to enable understanding of inhomogeneous flows, is examined in this paper for various deformations; steady-state shear flow, step strain, extension, and linear small amplitude oscillatory flow in homogeneous conditions. We also examine how systematic variations in the model parameters affect the rheological predictions and material functions.

Keywords: Wormlike micelles; Constitutive model; Viscoelastic flows; Larson model; Cates model

1. Introduction

Wormlike micelles, also known as living polymers, have been the center of numerous theoretical and experimental studies, see for example the reviews [1,2]. Unlike typical polymers these long macromolecular assemblies can break and reform continuously, showing distinctive behaviors under different deformation conditions. Observations in small amplitude oscillatory shear (SAOS) flows show that under certain conditions the linear viscoelastic response is primarily a single mode Maxwell response [3,4]. Specifically, if we denote τ_{break} as the expected time for breakage of the micelle, and $\tau_{\text{reptation}}$ as the expected time for a micelle to reptate out of its entanglements, when $\tau_{\text{break}} \ll \tau_{\text{reptation}}$, Cates [5], showed that wormlike micellar mixtures have a single mode Maxwellian response in the linear viscoelastic regime, with a second 'Rouse' mode important only at high frequencies. He also showed that the time scale associated with this first, dominant, mode is $\tau_{\text{eff}} = (\tau_{\text{reptation}}\tau_{\text{break}})^{1/2}$ [5,6]. In steady-state shear experiments, at small shear rates, $\dot{\gamma} < \dot{\gamma}_1$, and large shear rates, $\dot{\gamma} > \dot{\gamma}_2$, these micellar solutions exhibit a linear dependence of the stress on the shear rate. However, given the right conditions of concentration, salinity, and temperature [7], a stress plateau in an intermediate shear-rate region, $\dot{\gamma}_1 < \dot{\gamma} < \dot{\gamma}_2$, is observed in the flow curve and, in these cases, experiments in a circular Couette cell commonly show the formation of two primary 'shear bands', a high shear rate region near the inner or moving wall connected to a low shear rate region near the outer or fixed wall [8–10].

In uniaxial extension flows experiments have shown a plateau in the extensional viscosity for small extensional rates, followed by a sharp extensional thickening and, at a critical elongational rate, an extensional thinning [11].

In step strain these mixtures show a factorization of the shear stress as $\sigma_{r\theta} = \gamma G_0 g(t) h(\gamma)$ where $G(t) = G_0 g(t)$ is the stress relaxation modulus and $h(\gamma)$ the damping function. Experiments have shown that $G(t)$ can be well described by single exponential relaxation $G(t) = G_0\, \mathrm{e}^{-t/\lambda}$. The damping function may have a more complex response. Experiments by Brown et al. [12] on a CTAB/NaSal system show a strain-hardening response followed by a strain-softening. Recent experiments with a CPyCl/NaSal solution show a monotonic softening response similar to that described by the Doi–Edwards model [13]. Additionally, experiments show that the Lodge–Meissner relation is obeyed up to strains of $\gamma_0 \sim 8$ [13].

The present work presents a constitutive model to describe the flow of wormlike micellar solutions under these different

* Corresponding author. Tel.: +1 302 831 0582.
E-mail address: vasquez@math.udel.edu (P.A. Vasquez).

0377-0257/$ – see front matter © 2007 Elsevier B.V. All rights reserved.
doi:10.1016/j.jnnfm.2007.03.007

deformation conditions and details the rheological predictions and parameter dependence of the model. The model includes scission and reformation effects as well as an elastic network response and diffusion of species in the presence of stress gradients. Such a model should thus be capable of capturing inhomogeneous flow structures such as shear bands.

Various approaches have been taken in modeling wormlike micellar solutions. Cates [14] introduced reaction dynamics to account for the reversible breaking and reforming of the micellar chains. In his model there are two different time scales, the reptation time and the breaking time. Although experiments have shown good agreement with his model, especially in linear deformations, that model still fails to predict stress overshoot in the start up of steady shear [6] and to our knowledge no calculations in extensional flow have been done for that model. Other authors have combined dumbbell models for elastic chains and network theory by introducing creation and destruction terms in the evolution equation of the dumbbells [15,16]. Different forms of these breaking and reforming terms have been considered. Bautista et al. [17] developed a single species model based on a codeformational Maxwell constitutive equation and included a kinetic equation governing the relaxation time to account for the dependence of the breakage rate on the shear rate. This particular version of their model predicts a multivalued shear stress versus shear rate curve and hence one expects that the model will demonstrate shear banding.

Two species models have been considered to describe closely related fluids such as associative polymeric networks. These mixtures do not typically exhibit shear banding, but these models do incorporate two species in an elastic network with attachment and detachment of strands. In [18] Cates introduced a modified version of his association and dissociation dynamics [14], to model pairwise associating polymers. The dynamics discussed in that paper are similar to the ones considered here in that monomers form dimers and dimers break into monomers. In [18] Cates focuses primarily on computing terminal relaxation times. Using Brownian dynamics simulations to evaluate the rheological behavior of reversible polymeric networks, van den Brule and Hoogerbrugge [19] assumed that the probability of attachment to the network is proportional to the stretch of the dumbbell. They introduced a FENE-like term in the probability of detachment to account for the fact that during flow a chain has a higher probability of detaching once it becomes more fully stretched. Brownian dynamics were also used in the work of Hernandez-Cifre et al. [16] to simulate reversible polymeric networks, they considered two separate species, one representing active chains connected to the network by both ends, and the other representing dangling chains connected to the network by one end only. In their work, disassociation from the network was an exponential function of stress and, by using the same form of the association rate as [19] they were able to predict shear thickening. Tripathi et al. [20] in their two species network model for associative polymers derived a destruction rate for the non-linearly elastic bridging chains which depends on the stress acting on the micellar junction and a creation rate which depends on the configuration of the dangling ends and the local shear rate. In their work the creation rate of the bridging chains was proportional to a function of the shear rate and stress.

Single species bead–spring models based on the Johnson–Segalman constitutive equation were considered by Olmsted and collaborators. In these models the number density of the species was kept fixed and numerical studies were carried out with and without non-local diffusion terms [21–23]. A similar model but with addition of variable density was considered in Refs. [24,25]. These models result in a non-monotone stress–strain rate curve under homogeneous flow conditions. Under inhomogeneous flow conditions, with the addition of a viscous solvent and the incorporation of stress diffusion terms, these models predict a stress plateau in the flow curve over a range of shear rates. Numerical studies have shown that, without diffusion, the structure of the steady-state solution depends on the flow history [21]. For shear rates within the plateau region, these models predict shear banding in the velocity profiles across the gap in a cylindrical Couette geometry. Such models are phenomenological, that is they do not relate the state of the stress directly to the microstructural dynamics of the micellar system. Additionally, the Johnson–Segalman model predicts a singularity in the extensional viscosity at a finite elongational rate and exhibits a non-physical negative damping in rapid step strain deformations [26]. Experiments using NMR imaging [27] and small-angle neutron scattering [28] have also shown that for a model to be able to accurately describe the highly non-linear behavior of some wormlike micellar solutions, it should include local effects in the orientation and dynamics of the molecules, as opposed to a bulk average of the properties. For these reasons alternative models, tied to the physics of the micellar breakage and reforming processes, need to be considered.

The present approach is based on a discrete version of Cates' original reversible breaking theory. In contrast to Cates' model in which reptation theory was used, the breaking and reforming dynamics in this model are incorporated into network theory in which we follow elastic segments of wormy micelles between entanglement points. In the present approach two different species are considered, one of length L that breaks in the middle to form two strands of equal length, $L/2$. These strands can also recombine to form one species of length L as shown in Fig. 1.

In this paper we formulate the constitutive equations for such a model and consider predictions under different deformation conditions assuming homogeneous flow. In Section 2 we present the formulation and appropriate non-dimensionalization of our model. In Section 3 the governing equations describing steady and transient shear flow in a cylindrical Couette geometry and in uniaxial extensional flows are presented. Section 4 deals with analysis of the model in the linear viscoelastic regime, specifically small amplitude oscillation. Also, a first examination of the model parameters and their effects on the model predictions and in particular on the magnitude of the zero shear rate viscosity is presented. In Section 5 non-linear material functions in step strain, and in steady homogenous shear and elongational flow are studied. The dependency of the material functions on model parameters such as the equilibrium number density of

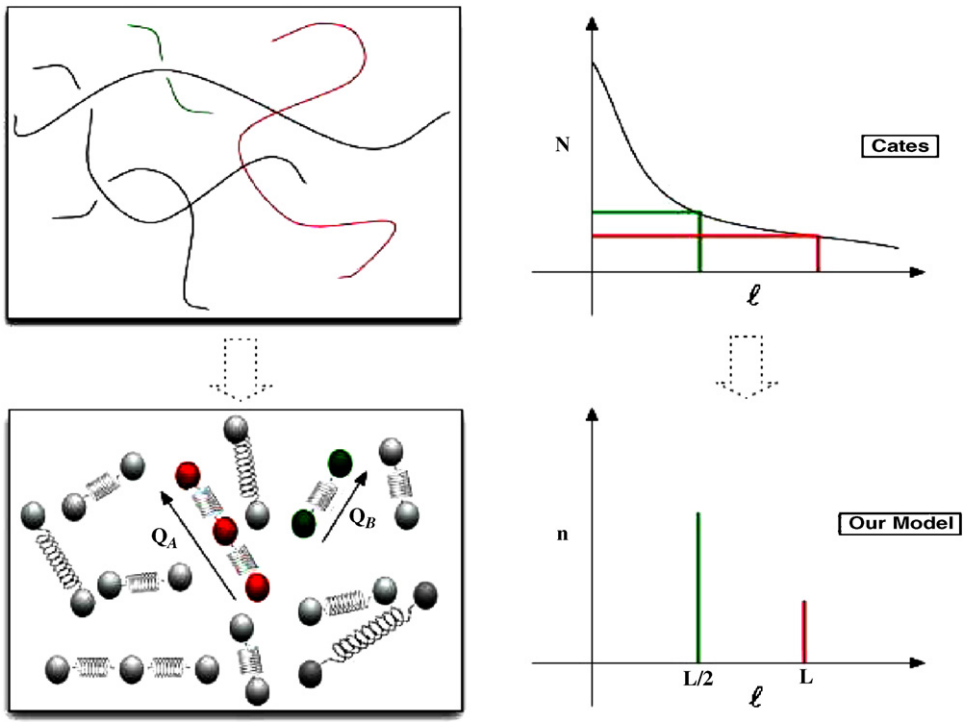

Fig. 1. Micellar network: (top) Cates' model with a continuous distribution of lengths $N(L)$ and (bottom) our discrete two species model.

each species and the breakage rate are explored. A second paper, Part II [13], consists of a detailed comparison of experiments with the predictions of the model and optimal model parameter selection for the model in agreement with experiments. Further papers analyze this and similar models computationally in steady and transient inhomogeneous shearing flows [29].

2. Formulation of the model

In the model presented here we simplify Cates' dynamics by considering only two species of wormlike micelles. We consider species A, which are chains of length L units that break at the middle to form chains of length $L/2$ units, denoted species B. Analogously, the short chains can join at their ends to reform into one long chain. This discrete dynamics is opposed to Cates' theory in which chains can break with equal probability at any point along their length, and in which chains of any length can join to form a longer chain. This simplification of Cates' breakage dynamics allows us to understand the species interaction, to examine the model in a variety of non-linear flow conditions, and in particular, to develop a theory which consistently captures the spatial variations in the number density of each species. This is key to understanding the experimental behavior of wormlike micellar solutions and the selection of the stress at which these solutions show shear banding [30]. One effect the continuous, versus the discrete, dynamics has on our results is that by allowing the chains to break at any point, the rate of breakage is effectively increased and the breakage time correspondingly decreased.

Let $\Psi'_A(\mathbf{r}', \mathbf{Q}', t')$, $\Psi'_B(\mathbf{r}', \mathbf{Q}', t')$ represent the number density distribution of each species in space, configuration space and time. Here $\mathbf{Q}'$ is the end to end vector of the chain. Then,

$$n'_\alpha(\mathbf{r}', t') = \int \Psi'_\alpha \, \mathrm{d}\mathbf{Q}'$$

represents the dimensional number density of species α as a function of space and time. Here and throughout this paper primes represent dimensional variables.

The equations governing the configuration density function, using network theory coupled with bead–spring kinetics, and assuming Hookean forces, can be obtained by generalizing techniques introduced by Bird et al. [31] and others [32,33] and used in Refs. [24,25], to formulate a two species model:

$$\Psi'_{A,t'} + \nabla_{\mathbf{r}'} \cdot (\mathbf{v}'_A \Psi'_A) + \nabla_{\mathbf{Q}'}(\mathbf{Q}' \cdot \nabla \mathbf{v}'_A)\Psi'_A - \nabla_{\mathbf{r}'} \cdot \frac{kT}{2\zeta_A} \nabla_{\mathbf{r}'} \Psi'_A + \nabla_{\mathbf{Q}'} \cdot \frac{2H_A}{\zeta_A} \mathbf{Q}' \Psi'_A - \nabla_{\mathbf{Q}'} \frac{2kT}{\zeta_A} \nabla_{\mathbf{Q}'} \Psi'_A = \frac{c_{B'}}{2} \Psi'_B * \Psi'_B - c_{A'} \Psi'_A \tag{1a}$$

$$\Psi'_{B,t'} + \nabla_{\mathbf{r}'} \cdot (\mathbf{v}'_B \Psi'_B) + \nabla_{\mathbf{Q}'}(\mathbf{Q}' \cdot \nabla \mathbf{v}'_B)\Psi'_B - \nabla_{\mathbf{r}'} \cdot \frac{kT}{2\zeta_B} \nabla_{\mathbf{r}'} \Psi'_B + \nabla_{\mathbf{Q}'} \cdot \frac{2H_B}{\zeta_B} \mathbf{Q}' \Psi'_B - \nabla_{\mathbf{Q}'} \frac{2kT}{\zeta_B} \nabla_{\mathbf{Q}'} \Psi'_B = -c'_B \Psi'_B * \Psi'_B + 2c'_A \Psi'_A \tag{1b}$$

In these equations k is the Boltzmann constant; T the temperature; ζ_α the drag coefficient of the species α; c'_A the dimensional breakage rate; c'_B the dimensional reforming rate per micelle; H_α is the spring constant or elasticity of the α th species.

The flux of species A and B relative to the main flow is given by

$$\mathbf{j}'_A = -\frac{kT}{\zeta_A}\nabla'\rho'_A + \frac{2mH_A}{\zeta_A}\nabla'\cdot\{\mathbf{Q}'\mathbf{Q}'\}_A, \tag{2a}$$

$$\mathbf{j}'_B = -\frac{kT}{\zeta_B}\nabla'\rho'_B + \frac{mH_B}{\zeta_B}\nabla'\cdot\{\mathbf{Q}'\mathbf{Q}'\}_B. \tag{2b}$$

The second term on the right hand side of Eq. (2) arises from assuming there is a finite spatial extent for the dumbbell that characterizes the elastic network segment and the mass is distributed at the two ends, one bead at $(\mathbf{r}' + (\mathbf{Q}'/2), \mathbf{Q}', t')$ and the other at $(\mathbf{r}' - (\mathbf{Q}'/2), \mathbf{Q}', t')$ [24,32,33].

By integrating the Smoluchowski equation (1) over $\mathbf{Q}'$, with $\rho'_A = 4mn'_A$ and $\rho'_B = 2mn'_B$, we obtain the evolution equations governing the number densities of each species,

$$\frac{Dn'_A}{Dt'} = -\frac{\nabla'\cdot\mathbf{j}'_A}{4m} + \frac{c'_B}{2}n'^2_B - c'_A n'_A, \tag{3a}$$

$$\frac{Dn'_B}{Dt'} = -\frac{\nabla'\cdot\mathbf{j}'_B}{2m} - c'_B n'^2_B + 2c'_A n'_A. \tag{3b}$$

The functional form of the reaction rates, c'_A, c'_B, for the breaking and reforming of the chains will be discussed in Section 2.3. For now we assume they are functions of the average extension of the respective chains and the shear rate:

$$c'_A(n'_A, \{\mathbf{Q}'\mathbf{Q}'\}_A, \dot{\boldsymbol{\gamma}}'), \qquad c'_B(n'_B, \{\mathbf{Q}'\mathbf{Q}'\}_B, \dot{\boldsymbol{\gamma}}').$$

Substituting for the flux from Eq. (2) into (3), the equations for the number density for each species become

$$\frac{Dn'_A}{Dt'} = 2D_A\nabla'^2 n'_A - \frac{D_A H_A}{kT}\nabla'\nabla' : \{\mathbf{Q}'\mathbf{Q}'\}_A + \frac{c'_B}{2}n'^2_B - c'_A n'_A, \tag{4a}$$

$$\frac{Dn'_B}{Dt'} = 2D_B\nabla'^2 n'_B - \frac{D_B H_B}{kT}\nabla'\nabla' : \{\mathbf{Q}'\mathbf{Q}'\}_B - c'_B n'^2_B + 2c'_A n'_A. \tag{4b}$$

Here the diffusivities of the A and B chains are $D_A = kT/2\zeta_A$, $D_B = kT/2\zeta_B$, respectively. The stress associated with the α th species is related to the second moment of the distribution by

$$\{\mathbf{Q}'\mathbf{Q}'\}_\alpha = \int \mathbf{Q}'\mathbf{Q}'\Psi'_\alpha \,\mathrm{d}\mathbf{Q}'. \tag{5}$$

Then multiplying the distribution Eq. (1) by $\mathbf{Q}'\mathbf{Q}'$ and integrating over the configuration space, $\mathrm{d}\mathbf{Q}'$, we find the equations for the second moment of each species:

$$\{\mathbf{Q}'\mathbf{Q}'\}_{A(1')} + \frac{4H_A}{\zeta_A}\{\mathbf{Q}'\mathbf{Q}'\}_A - \frac{4n'_A kT}{\zeta_A}\mathbf{I} - D_A\nabla'^2\{\mathbf{Q}'\mathbf{Q}'\}_A = \frac{c'_B}{2}\{\mathbf{Q}'\mathbf{Q}'\}_B n'_B - c'_A\{\mathbf{Q}'\mathbf{Q}'\}_A, \tag{6a}$$

$$\{\mathbf{Q}'\mathbf{Q}'\}_{B(1')} + \frac{4H_B}{\zeta_B}\{\mathbf{Q}'\mathbf{Q}'\}_B - \frac{4n'_B kT}{\zeta_B}\mathbf{I} - D_B\nabla'^2\{\mathbf{Q}'\mathbf{Q}'\}_B = -c'_B\{\mathbf{Q}'\mathbf{Q}'\}_B n'_B + 2c'_A\{\mathbf{Q}'\mathbf{Q}'\}_A, \tag{6b}$$

where $(\cdot)_{(1')}$ represents the upper convected time derivative defined as

$$(\cdot)_{(1')} = \frac{D}{Dt'}(\cdot) - (\nabla'\mathbf{v}')^{\mathrm{T}}\cdot(\cdot) - (\cdot)\cdot(\nabla'\mathbf{v}').$$

Because the flow may be inhomogeneous, that is the number density distribution function, Ψ'_α, of each species varies in space, configuration space and time, the number densities, $n'_\alpha(\mathbf{r}, t)$, cannot be factored out of the second moment, and

$$\{\mathbf{Q}'\mathbf{Q}'\}_\alpha \neq n'_\alpha\langle\mathbf{Q}'\mathbf{Q}'\rangle_\alpha.$$

Finally, the total micellar contribution to the stress is given by

$$\boldsymbol{\sigma}' = H_A\{\mathbf{Q}'\mathbf{Q}'\}_A + H_B\{\mathbf{Q}'\mathbf{Q}'\}_B. \tag{7}$$

2.1. Non-dimensionalization

The equations are non-dimensionalized as follows:

$$\mathbf{r} = \frac{\mathbf{r}'}{d}, \qquad t = \frac{t'}{\lambda_{\mathrm{eff}}}, \qquad \mathbf{v} = \mathbf{v}'\frac{\lambda_{\mathrm{eff}}}{\mathrm{d}}d,$$

$$\{\mathbf{QQ}\}_\alpha = \frac{H_A\{\mathbf{Q}'\mathbf{Q}'\}_\alpha}{n'^0_A kT}, \qquad n_\alpha = \frac{n'_\alpha}{n'^0_A},$$

where $\alpha = A, B$; d is a macroscopic characteristic length, in circular Couette geometry, $d = R_\mathrm{o} - R_\mathrm{i}$ where R_o, R_i are the outer and inner radii; λ_{eff} is the effective relaxation time of the network (to be determined); and $\sqrt{n'^0_A kT/H_A}$ is a characteristic microscopic length scale for an elastic segment of species A. Here n'^0_A is the dimensional value of the number density of chains of length L at equilibrium conditions. The relaxation time of the α th species is $\lambda_\alpha = \zeta_\alpha/4H_\alpha$. As opposed to being located solely at the beads, as in bead–spring dumbbell models, the drag is distributed along the chain, in accordance with network theory, and hence depends non-linearly on the molecular weight of the chain.

As will be seen through fitting to experimental data, the shorter chains have a much shorter relaxation time, λ_B, than that of the longer chains, λ_A. Note that, since we only consider two species, we effectively lump "all" short segments as species B and "all" long entangled chains as species A. Then, from reptation theory [34], one would expect that $\lambda_A \sim L^3/L_\mathrm{E}$ where L_E is the entanglement length [6]. On the other hand, the lumped species B represents short segments with a Rouse-like relaxation mechanism, so that $\lambda_B \sim (L/2)^2$ [6]. Thus we expect,

$$\frac{\lambda_A}{\lambda_B} \sim 4\frac{L}{L_\mathrm{E}} \gg 1, \tag{8}$$

hence, after the values of λ_A and λ_B are determined, the ratio in Eq. (8) should be an indicator of how long and/or entangled the chains are in the system.

The consideration of only two species simplifies the analysis but it is also restrictive. Introduction of more species enables

us to capture the distribution of chain lengths and a broader spectrum of relaxation times as observed in wormlike micellar solutions, but it substantially complicates the analysis.

For compactness, we define the two configuration tensors

$$\mathbf{A} = \int \mathbf{QQ}\Psi_A \, \mathrm{d}\mathbf{Q} = \{\mathbf{QQ}\}_A, \tag{9a}$$

$$\mathbf{B} = \int \mathbf{QQ}\Psi_B \, \mathrm{d}\mathbf{Q} = \{\mathbf{QQ}\}_B. \tag{9b}$$

Additionally, the dimensionless breakage and reformation rates are given by

$$c_A = \lambda_A \, c'_A, \qquad c_B = \lambda_A n'^0_A c'_B, \tag{10}$$

where c_A is the ratio of the relaxation time of the long chains to the breakage time of the long chain, similarly for c_B and the shorter chains. The ratio of the relaxation time of the short chains to the relaxation time of the long chains is denoted by

$$\epsilon = \frac{\lambda_B}{\lambda_A}, \tag{11}$$

and that of the relaxation time of the long chains to the effective relaxation time of the elastic network, as

$$\mu = \frac{\lambda_A}{\lambda_{\mathrm{eff}}}. \tag{12}$$

The ratio of the spring constant of the shorter chains to that of the longer chains is

$$\frac{H_B}{H_A} = H^*. \tag{13}$$

If the network segments are ideal Hookean entropic springs, then we expect

$$H_B = \frac{3kT}{l^2 N_B} \quad \text{and} \quad H_A = \frac{3kT}{l^2 N_A} = \frac{3kT}{2l^2 N_B},$$

where N_α is the number of Kuhn steps of length l in the segment of species α. Note that, in our two species model, $N_A = 2N_B$ so $H^* = 2$. The ratios ϵ, μ are to be determined by fitting to experiments.

Finally, the non-dimensional total stress $\boldsymbol{\sigma}$ is given by

$$\boldsymbol{\sigma} = \frac{\boldsymbol{\sigma}'}{G_0} = \{\mathbf{QQ}\}_A + H^*\{\mathbf{QQ}\}_B = \mathbf{A} + 2\mathbf{B} \tag{14}$$

where $G_0 = n'^0_A kT$ is a characteristic elastic modulus arising from the long, A, chains.

2.2. Governing equations

With the scaling and parameters introduced in Section 2.1, Eqs. (4)–(6) become

$$\mu \frac{Dn_A}{Dt} = 2\delta_A \nabla^2 n_A - \delta_A \nabla\nabla : \mathbf{A} + \frac{1}{2} c_B n_B^2 - c_A n_A, \tag{15a}$$

$$\mu \frac{Dn_B}{Dt} = 2\delta_B \nabla^2 n_B - 2\delta_B \nabla\nabla : \mathbf{B} - c_B n_B^2 + 2c_A n_A, \tag{15b}$$

$$\mu \mathbf{A}_{(1)} + \mathbf{A} - n_A \mathbf{I} - \delta_A \nabla^2 \mathbf{A} = c_B n_B \mathbf{B} - c_A \mathbf{A}, \tag{16a}$$

$$\epsilon\mu \mathbf{B}_{(1)} + \mathbf{B} - \frac{n_B}{2}\mathbf{I} - \epsilon\delta_B \nabla^2 \mathbf{B} = -2\epsilon c_B n_B \mathbf{B} + 2\epsilon c_A \mathbf{A}, \tag{16b}$$

Here, we have defined non-dimensional diffusion constants $\delta_\alpha = \lambda_A D_\alpha / d^2$ for $\alpha = A, B$.

These equations for the number density and stress must be coupled with the fluid equations of conservation of mass, and of conservation of momentum:

$$\nabla \cdot \mathbf{v} = 0, \tag{17}$$

$$E^{-1} \frac{D\mathbf{v}}{Dt} = \nabla \cdot \boldsymbol{\Pi}, \tag{18}$$

where E is an elasticity number defined as

$$E = \frac{G_0 \lambda_{\mathrm{eff}}^2}{\rho d^2} = \frac{De}{Re}. \tag{19}$$

Here $Re = \rho V' d/\eta'_0$ is the Reynolds number and $De = \lambda_{\mathrm{eff}} V'/d$ is the Deborah number, where V' is the velocity at the moving wall. Thus, with our scaling, the dimensionless value of the velocity at the moving boundary is De. The dimensionless diffusion constants are

$$\delta_A = \frac{\lambda_A D_A}{d^2} = \frac{\lambda_A V'}{d} \cdot \frac{D_A}{V' d} = \frac{De}{Pe},$$

$$\delta_B = \frac{\zeta_A}{\zeta_B}\delta_A = \frac{1}{2\epsilon}\frac{De}{Pe},$$

where the Peclet number is $Pe = V' d/D_A$ and is a measure of the relative importance of convection to diffusion of the elastic chains of species A.

In addition, the total stress tensor is given by

$$\boldsymbol{\Pi} = p\mathbf{I} - \beta\dot{\boldsymbol{\gamma}} + \boldsymbol{\tau}, \tag{20}$$

where the extra stress arising from the network is

$$\boldsymbol{\tau} = (n_A + n_B)\mathbf{I} - (\mathbf{A} + 2\mathbf{B}), \tag{21}$$

and the solvent contribution to the total viscosity is $\beta = \eta_{\mathrm{s}}/\eta'_0$, where η_{s} is the solvent viscosity, and η'_0 is the dimensional zero shear rate viscosity.

To solve the system of Eqs. (17)–(21), appropriate boundary and initial conditions on both stress and velocity need to be specified. In this paper spatial variations are not considered, thus boundary conditions for stress are not required at this point. A full discussion of boundary conditions will be given in Part III [29], where the full inhomogeneous flow is solved numerically.

On the other hand, initial values are found from Eqs. (15)–(16) assuming equilibrium conditions. That is, in absence of flow, $n_A^0 = 1$ and Eq. (15a) gives

$$n_B^0 = \sqrt{\frac{2c_{A_{\mathrm{eq}}}}{c_{B_{\mathrm{eq}}}}}, \tag{22}$$

where $c_{A_{\mathrm{eq}}}, c_{B_{\mathrm{eq}}}$ are the values of the breakage and reformation rates c_A, c_B at equilibrium.

Similarly, at equilibrium we obtain

$$\mathbf{A}_{\mathrm{eq}} = \mathbf{I}, \qquad \mathbf{B}_{\mathrm{eq}} = \frac{n_B^0}{2}\mathbf{I}.$$

2.3. Determination of breakage rate

So far we have developed a general two species network model for the evolution of stress and number density of elastic segments of length Q_A, Q_B. To complete the model we need to specify appropriate breakage and reformation rates that describe the evolution of the number density of each species under both equilibrium and flowing conditions. In principle, appropriate expressions could be determined by Brownian dynamics calculations of entangled wormlike micelles in the same manner as the studies of van den Brule and Hoogerbrugge [19] and Hernandez-Cifre et al. [16] for associative polymer networks. However, such simulations are complicated by the multiple breaking and reforming events expected for each chain. In the present work we thus use simplified analytic expressions for each term. In particular, the dependence of the breakage rate of the elastically active network elements (which correspond to stretched micellar segments) on the flow strength is taken to be of the form of the tube loss term, proposed by Larson [35]. In this work Larson considered the dynamics of network segments which are convected by a flow but which do not deform affinely inside their bounding tubes. The resulting partially extending convected (PEC) strand model provides a simple differential analog of the Doi–Edwards reptation theory. The longer elastic segments, species A, in our model will experience similar convection by the flow and recoil following a breakage event before being reincorporated into the network. We thus write

$$c_A = c_{A_{\mathrm{eq}}} + \frac{1}{3}\xi\mu\left(\dot{\boldsymbol{\gamma}} : \frac{\mathbf{A}}{n_A}\right), \tag{23a}$$

$$c_B = c_{B_{\mathrm{eq}}}. \tag{23b}$$

A term with similar functional form to that in our breaking term is used in the single species differential model of Marrucci et al. [36] and in Likhtman and Graham's non-extendable limit of their Rolie-Poly model [37]. Although in the latter two cases full retraction of the strand within the tube is assumed, in the Larson's form the parameter ξ is allowed to vary to capture the partial retraction of a strand within its tube. When $\xi = 0$ this corresponds to no retraction or ideal affine neo-Hookean behavior, the resulting constitutive equation is of simple convected Maxwell form [31]. When $\xi \neq 0$ this corresponds to partial extension and retraction. Finally, when $\xi = 3/5$ Larson showed that the PEC model closely approximates the Doi–Edwards theory in which the chain fully retracts inside the deforming tube.

Larson's term, which represents tube breakage after partial retraction, is used instead in our case to model stress-induced micelle breakage. We have introduced this term as an explicit breakage term in our two species model as opposed to a non-affine derivative in a single species model, as introduced by Larson. Thus the non-affine nature of our network deformation arises due to the continued breaking and the reforming of the elastic elements comprising the network. When the breaking and reforming rates are set to zero the model reduces to two uncoupled Maxwell modes, which agrees with the observations in linear regimes, so that the non-linear behavior of wormlike micellar solutions in this model comes from the breaking and reforming terms.

The advantage of the Larson-type term in the single species case, provided a solvent viscosity is added to the model similar to the Johnson–Segalman model, is that it not only predicts a non-monotonic flow curve (which may result in shear-banding), but that also, unlike the Johnson–Segalman model, it obeys the Lodge–Meissner relation in step strain and it exhibits a maximum in elongational viscosity as a function of elongation rate [26]. The single species model proposed by Larson has shown good agreement with experimental data in shear, extensional, and step strain for certain polymeric melts, although it was noted that different values of the parameter ξ are needed to quantitatively describe each type of deformation [26,38].

A similar expression to the one in Eq. (23a), is also used in the two species network model of Tripathi et al. [20] for associative polymer networks in order to describe the creation rate of bridging chains from dangling chains. The difference between that model and the model presented here is that our model incorporates inhomogeneities in the flow, and that Tripathi et al. explicitly modeled the molecular weight dependence of the breaking rate of the bridging chains, which we have not included. In addition, the creation and destruction of each species is modeled as a first order reaction in the Tripathi case, whereas the creation rate of long chains is quadratic in our model as it inherently involves the combination of two shorter chains rather than the reincorporation of a dangling chain into an elastic network.

3. Predictions in viscometric flow

Experiments with wormlike micellar solutions carried out in cylindrical Couette devices show that spatial variations develop in the flow above a critical shear rate [8,10,28,39]. We consider Eqs. (15) and (16) in the absence of spatial variation, thus we assume $\delta_A = \delta_B = 0$ and $\dot{\boldsymbol{\gamma}}$ (**r**)constant. Here, we present the formulation and rheological predictions of this two species micellar network model under such assumptions.

3.1. Shear flow in circular-Couette geometry

We employ the following assumptions of a homogeneous unidirectional shear flow,

$$\mathbf{v} = (0, v(r), 0), \qquad \mathbf{v}\cdot\nabla(\cdot) = 0, \qquad \dot{\boldsymbol{\gamma}} = \dot{\gamma}_0\boldsymbol{\delta}_r\boldsymbol{\delta}_\theta + \dot{\gamma}_0\boldsymbol{\delta}_\theta\boldsymbol{\delta}_r,$$
$$\dot{\boldsymbol{\gamma}} : \mathbf{A} = 2\dot{\gamma}_0 A_{r\theta},$$

and substitute these in Eqs. (15) and (16) to find evolution equations for the number densities and stress contributions, from species A and B, as functions of $\dot{\gamma}_0$. Note that in non-viscometric flow spatial variations arise through the shear rate, $\dot{\gamma} = r\partial(v/r)/\partial r$. We thus obtain the following expressions for the number density of each species:

$$\mu\frac{\mathrm{d}n_A}{\mathrm{d}t} = \frac{1}{2}c_{B_{\mathrm{eq}}}n_B^2 - \frac{2}{3}\xi\mu\dot{\gamma}_0 A_{r\theta} - c_{A_{\mathrm{eq}}}n_A, \tag{24a}$$

$$\mu\frac{\mathrm{d}n_B}{\mathrm{d}t} = -c_{B_{\mathrm{eq}}}n_B^2 + \frac{4}{3}\xi\mu\dot{\gamma}_0 A_{r\theta} + 2c_{A_{\mathrm{eq}}}n_A \tag{24b}$$

and for the components of the stress tensor $\mathbf{A}$ for species A:

$$\mu\frac{\mathrm{d}A_{rr}}{\mathrm{d}t}+A_{rr}-n_A=c_{B_{\mathrm{eq}}}n_BB_{rr}-\frac{2}{3}\xi\mu\dot{\gamma}_0\frac{A_{r\theta}}{n_A}A_{rr}-c_{A_{\mathrm{eq}}}A_{rr}, \tag{25a}$$

$$\mu\frac{\mathrm{d}A_{r\theta}}{\mathrm{d}t}-\mu\dot{\gamma}_0A_{rr}+A_{r\theta}=c_{B_{\mathrm{eq}}}n_BB_{r\theta}-\frac{2}{3}\xi\mu\dot{\gamma}_0\frac{A_{r\theta}}{n_A}A_{r\theta}-c_{A_{\mathrm{eq}}}A_{r\theta}, \tag{25b}$$

$$\mu\frac{\mathrm{d}A_{\theta\theta}}{\mathrm{d}t}-2\mu\dot{\gamma}_0A_{r\theta}+A_{\theta\theta}-n_A=c_{B_{\mathrm{eq}}}n_BB_{\theta\theta}-\frac{2}{3}\xi\mu\dot{\gamma}_0\frac{A_{r\theta}}{n_A}A_{\theta\theta}-c_{A_{\mathrm{eq}}}A_{\theta\theta}, \tag{25c}$$

$$\mu\frac{\mathrm{d}A_{zz}}{\mathrm{d}t}+A_{zz}-n_A=c_{B_{\mathrm{eq}}}n_BB_{zz}-\frac{2}{3}\xi\mu\dot{\gamma}_0\frac{A_{r\theta}}{n_A}A_{zz}-c_{A_{\mathrm{eq}}}A_{zz} \tag{25d}$$

and finally for the stress associated with species B:

$$\epsilon\mu\frac{\mathrm{d}B_{rr}}{\mathrm{d}t}+B_{rr}-\frac{1}{2}n_B=\epsilon\left[-2c_{B_{\mathrm{eq}}}n_BB_{rr}+\frac{4}{3}\xi\mu\dot{\gamma}_0\frac{A_{r\theta}}{n_A}A_{rr}+2c_{A_{\mathrm{eq}}}A_{rr}\right], \tag{26a}$$

$$\epsilon\mu\frac{\mathrm{d}B_{r\theta}}{\mathrm{d}t}-\epsilon\mu\dot{\gamma}_0B_{rr}+B_{r\theta}=\epsilon\left[-2c_{B_{\mathrm{eq}}}n_BB_{r\theta}+\frac{4}{3}\xi\mu\dot{\gamma}_0\frac{A_{r\theta}}{n_A}A_{r\theta}+2c_{A_{\mathrm{eq}}}A_{r\theta}\right], \tag{26b}$$

$$\epsilon\mu\frac{\mathrm{d}B_{\theta\theta}}{\mathrm{d}t}-2\epsilon\mu\dot{\gamma}_0B_{r\theta}+B_{\theta\theta}-\frac{1}{2}n_B=\epsilon\left[-2c_{B_{\mathrm{eq}}}n_BB_{\theta\theta}+\frac{4}{3}\xi\mu\dot{\gamma}_0\frac{A_{r\theta}}{n_A}A_{\theta\theta}+2c_{A_{\mathrm{eq}}}A_{\theta\theta}\right], \tag{26c}$$

$$\epsilon\mu\frac{\mathrm{d}B_{zz}}{\mathrm{d}t}+B_{zz}-\frac{1}{2}n_B=\epsilon\left[-2c_{B_{\mathrm{eq}}}n_BB_{zz}+\frac{4}{3}\xi\mu\dot{\gamma}_0\frac{A_{r\theta}}{n_A}A_{zz}+2c_{A_{\mathrm{eq}}}A_{zz}\right]. \tag{26d}$$

3.2. Extensional flow

For homogeneous uniaxial extensional flow with extension rate $\dot{\varepsilon}_0$ we have:

$$\mathbf{v}=(-\tfrac{1}{2}\dot{\varepsilon}_0r,0,\dot{\varepsilon}_0z),\qquad\mathbf{v}\cdot\nabla(\cdot)=0,$$
$$\dot{\boldsymbol{\gamma}}=-\dot{\varepsilon}_0\boldsymbol{\delta}_r\boldsymbol{\delta}_r-\dot{\varepsilon}_0\boldsymbol{\delta}_\theta\boldsymbol{\delta}_\theta+2\dot{\varepsilon}_0\boldsymbol{\delta}_z\boldsymbol{\delta}_z,$$
$$\dot{\boldsymbol{\gamma}}:\mathbf{A}=\dot{\varepsilon}_0(2A_{zz}-A_{rr}-A_{\theta\theta})=2\dot{\varepsilon}_0(A_{zz}-A_{rr}).$$

Eqs. (15) and (16) give for the number densities of species A and B:

$$\mu\frac{\mathrm{d}n_A}{\mathrm{d}t}=\frac{1}{2}c_{B_{\mathrm{eq}}}n_B^2-\frac{2}{3}\xi\mu\dot{\varepsilon}_0(A_{zz}-A_{rr})-c_{A_{\mathrm{eq}}}n_A, \tag{27a}$$

$$\mu\frac{\mathrm{d}n_B}{\mathrm{d}t}=-c_{B_{\mathrm{eq}}}n_B^2+\frac{4}{3}\xi\mu\dot{\varepsilon}_0(A_{zz}-A_{rr})+2c_{A_{\mathrm{eq}}}n_A \tag{27b}$$

and for the components of the stress tensor $\mathbf{A}$ for species A:

$$\mu\frac{\mathrm{d}A_{rr}}{\mathrm{d}t}+\mu\dot{\varepsilon}_0A_{rr}+A_{rr}-n_A=c_{B_{\mathrm{eq}}}n_BB_{rr}-\frac{2}{3}\frac{\xi\mu\dot{\varepsilon}_0}{n_A}(A_{zz}-A_{rr})A_{rr}-c_{A_{\mathrm{eq}}}A_{rr}, \tag{28a}$$

$$\mu\frac{\mathrm{d}A_{r\theta}}{\mathrm{d}t}+A_{r\theta}=c_{B_{\mathrm{eq}}}n_BB_{r\theta}-\frac{2}{3}\frac{\xi\mu\dot{\varepsilon}_0}{n_A}(A_{zz}-A_{rr})A_{r\theta}-c_{A_{\mathrm{eq}}}A_{r\theta}, \tag{28b}$$

$$\mu\frac{\mathrm{d}A_{zz}}{\mathrm{d}t}-2\mu\dot{\varepsilon}_0A_{zz}+A_{zz}-n_A=c_{B_{\mathrm{eq}}}n_BB_{zz}-\frac{2}{3}\frac{\xi\mu\dot{\varepsilon}_0}{n_A}(A_{zz}-A_{rr})A_{zz}-c_{A_{\mathrm{eq}}}A_{zz} \tag{28c}$$

and finally for the stress associated with species B:

$$\epsilon\mu\frac{\mathrm{d}B_{rr}}{\mathrm{d}t}+\epsilon\mu\dot{\varepsilon}_0B_{rr}+B_{rr}-\frac{1}{2}n_B=\epsilon\left[-2c_{B_{\mathrm{eq}}}n_BB_{rr}+\frac{4}{3}\frac{\xi\mu\dot{\varepsilon}_0}{n_A}(A_{zz}-A_{rr})A_{rr}+2c_{A_{\mathrm{eq}}}A_{rr}\right], \tag{29a}$$

$$\epsilon\mu\frac{\mathrm{d}B_{r\theta}}{\mathrm{d}t}+B_{r\theta}=\epsilon\left[-2c_{B_{\mathrm{eq}}}n_BB_{r\theta}+\frac{4}{3}\frac{\xi\mu\dot{\varepsilon}_0}{n_A}(A_{zz}-A_{rr})A_{r\theta}+2c_{A_{\mathrm{eq}}}A_{r\theta}\right], \tag{29b}$$

$$\epsilon\mu\frac{\mathrm{d}B_{zz}}{\mathrm{d}t}-2\epsilon\mu\dot{\varepsilon}_0B_{zz}+B_{zz}-\frac{1}{2}n_B=\epsilon\left[-2c_{B_{\mathrm{eq}}}n_BB_{zz}+\frac{4}{3}\frac{\xi\mu\dot{\varepsilon}_0}{n_A}(A_{zz}-A_{rr})A_{zz}+2c_{A_{\mathrm{eq}}}A_{zz}\right]. \tag{29c}$$

The equations for $A_{\theta\theta}$ and $B_{\theta\theta}$ are identical to those for A_{rr}, B_{rr}, respectively, with all rr components changed to $\theta\theta$ components. Note that if $A_{r\theta}$, $B_{r\theta}$ are initially zero, they stay identically zero. Hence this component of the stress does not play an important role in extensional flow except under pre-shear conditions in which $A_{r\theta}$, $B_{r\theta}$ may not be zero at the inception of the extensional flow. Recent experiments have considered the role of pre-shear on the extensional response of micellar networks [40], but analysis of this is beyond the scope of the present study.

4. Linear viscoelasticity

We now proceed to solve the constitutive equations to evaluate the steady and transient rheological predictions. We first consider the linearized limit of small deformations. In general, as will be seen below, fitting the linearized equations in shear to linear viscoelastic data only serves to determine the effective relaxation time of the network, $\lambda_{\mathrm{eff}}=\lambda_A/(1+c_{A_{\mathrm{eq}}})$, and

the product $\lambda_2 n_B^0 = \lambda_2\sqrt{2c_{A_{eq}}/c_{B_{eq}}}$. In order to fully determine the individual model parameters, in particular the magnitude of the equilibrium reaction rates, $c_{A_{eq}}$ and $c_{B_{eq}}$, non-linear deformations must be considered. The set of parameters specified above cannot be determined uniquely from the available linear viscoelastic data, due to the limitation of the ranges of frequencies obtained experimentally. The parameter ξ describes the non-linear breakage processes and can only be determined by regressing to full non-linear rheological measures.

4.1. Small amplitude oscillatory shear flow (SAOS)

In this section we develop linear theory in SAOS flow. Assuming that

$$\gamma_{r\theta} = \Re\mathrm{e}\{\gamma^0 \mathrm{e}^{\mathrm{i}\omega t}\} \quad \text{and} \quad \gamma^0 \ll 1,$$

where $\omega = \lambda_{\mathrm{eff}}\omega'$ is the dimensionless oscillation frequency, inserting this into Eqs. (24)–(26), and keeping only linear terms in γ^0 we obtain:

$$\mathrm{i}\mu\omega A_{r\theta}^1 + (1 + c_{A_{eq}})A_{r\theta}^1 - c_{B_{eq}} n_B^0 B_{r\theta}^1 = \mathrm{i}\mu\omega\gamma^0 A_{rr}^0, \tag{30a}$$

$$(1 + c_{A_{eq}})A_{rr}^0 - c_{B_{eq}} n_B^0 B_{rr}^0 = n_A^0 = 1, \tag{30b}$$

$$\mathrm{i}\epsilon\mu\omega B_{r\theta}^1 + B_{r\theta}^1(1 + 2\epsilon c_B n_B) - 2c_{A_{eq}}\epsilon A_{r\theta}^1 = \mathrm{i}\epsilon\mu\omega\gamma^0 B_{rr}^0, \tag{30c}$$

$$B_{rr}^0(1 + 2\epsilon c_{B_{eq}} n_B^0) = \tfrac{1}{2}n_B^0 + 2\epsilon c_{A_{eq}} A_{rr}^0, \tag{30d}$$

$$c_{B_{eq}} n_B^2 - 2c_{A_{eq}} = 0. \tag{30e}$$

Note that in linearized small disturbance theory the number density of each species, n_A^0 and n_B^0, are constant since variations in these terms are introduced in the full Eq. (24) by quadratically small terms. In these linearized equations all quantities are non-dimensional as before. Eqs. (30b) and (30d) give, after ignoring $O(\epsilon)$ terms,

$$B_{rr}^0 = \tfrac{1}{2}n_B^0, \tag{31a}$$

$$A_{rr}^0 = 1. \tag{31b}$$

Thus, for ϵ small, we have

$$A_{rr}^0 = 1, \tag{32a}$$

$$B_{rr}^0 = \tfrac{1}{2}n_B^0, \tag{32b}$$

$$A_{r\theta}^1 = \gamma^0\left(\frac{((\mu/(1 + c_{A_{eq}}))\omega)^2}{1 + ((\mu/(1 + c_{A_{eq}}))\omega)^2} + \frac{\mathrm{i}(\mu/(1 + c_{A_{eq}}))\omega}{1 + ((\mu/(1 + c_{A_{eq}}))\omega)^2}\right) + \cdots, \tag{32c}$$

$$B_{r\theta}^1 = \gamma^0\frac{n_B^0}{2}\left(\frac{(\epsilon\mu\omega)^2}{1 + (\epsilon\mu\omega)^2} + \frac{\mathrm{i}\epsilon\mu\omega}{1 + (\epsilon\mu\omega)^2}\right) + \cdots. \tag{32d}$$

In the limit of small frequencies the system behaves as a single mode Maxwellian system. Our system of equations has been non-dimensionalized by the effective relaxation time and hence we use Eq. (32c) to define the effective relaxation time, λ_{eff}, as

$$\lambda_{\mathrm{eff}} = \frac{\lambda_A}{1 + c_{A_{eq}}} = \frac{\lambda_A}{1 + \lambda_A c'_{A_{eq}}} = \frac{1}{\frac{1}{\lambda_A} + c'_{A_{eq}}}, \tag{33}$$

which results from setting the ratio $\mu/(1 + c_{A_{eq}})$ to unity. Here λ_{eff} has units of time.

Eq. (33) shows that the overall relaxation time of the network, λ_{eff}, is reduced from the longest relaxation time of the elastic chains, λ_A, due to the additional mechanism of breakage. Thus, the stress relaxes either through chains of length L relaxing or through the chains of length L breaking to form chains of length $L/2$. This re-scaling of the effective relaxation time is a result of the simplification of Cates' continuous breaking dynamics to a two species discrete limit. Recall that in the continuous limit Cates showed (in our notation) that $\lambda_{\mathrm{eff}} = (\lambda_A\lambda_{\mathrm{break}})^{1/2}$.

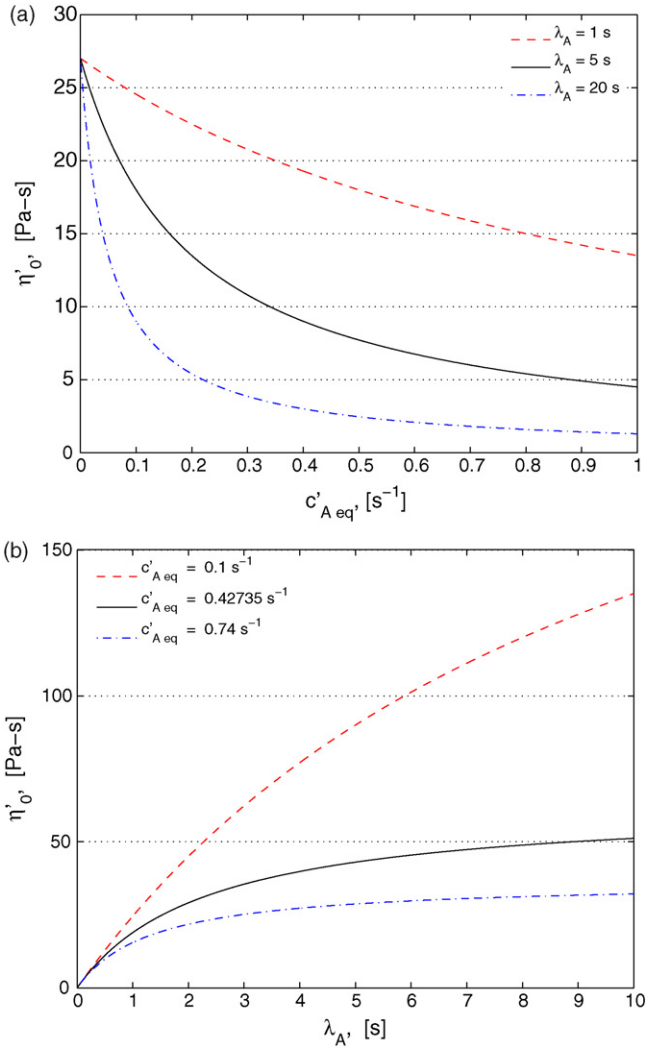

Fig. 2. Variations on the zero shear rate viscosity for: (a) different relaxation times of species A, λ_A, and (b) different breaking rates at equilibrium, $c'_{1_{eq}}$. In these figures, $G_0 = 27$ Pa.

Finally, for all values of ω the linear system behaves as the superposition of two Maxwell modes with relaxation times λ_{eff} and λ_B, respectively.

From these results the zero shear rate viscosity is given, to order ϵ, by

$$\eta_0' = n_A^0 kT \frac{\lambda_A}{1 + \lambda_A c'_{A_{\text{eq}}}} = G_0 \lambda_{\text{eff}}.$$

For a fixed relaxation time of the longer species, λ_A, the dimensional zero shear rate viscosity of the mixture decreases as the breaking rate at equilibrium, $c'_{A_{\text{eq}}}$, increases. The effective relaxation time also decreases as the breakage rate increases. Fig. 2 (a) shows the variation in the zero shear rate viscosity, η_0', as a function of the breakage rate $c'_{A_{\text{eq}}}$, for different values of λ_A. In Fig. 2(b), the breakage rate, $c'_{A_{\text{eq}}}$ is kept fixed at different values, and η_0' is plotted against λ_A. Experiments have shown that for a given solution the zero shear rate viscosity increases non-linearly with increasing surfactant concentration [9,41,42]. Hence in our model, the model parameters $c'_{A_{\text{eq}}}$ and λ_A play an important role in capturing the effect of concentration and salinity. That is, in order to change $c'_{A_{\text{eq}}}$ or λ_A one would need to change the concentration of polymer, the concentration of salt, and/or change the type of salt counterion.

5. Evaluation of model parameters

The characteristic stress scale for the micellar network is given by $G_0 = n'^0_A kT$. Following this non-dimensionalization, the response of a particular micellar solution to non-linear deformations is described in this model by three independent parameters. At first glance, the model appears to contain six parameters: λ_A, λ_B, $c_{A_{\text{eq}}}$, $c_{B_{\text{eq}}}$, n_B^0, and ξ. However, five of the parameters are related to one another through three independent equations. In the first of these we see from (15a) that the reaction rates $c_{A_{\text{eq}}}$, $c_{B_{\text{eq}}}$, and the number density of the second species n_B^0 are related by

$$n_B^0 = \sqrt{\frac{2c_{A_{\text{eq}}}}{c_{B_{\text{eq}}}}}.$$

Recall that the number densities were non-dimensionalized by n'^0_A so that $n_A^0 = 1$. Similarly, when the effective relaxation time of the solution, λ_{eff}, is known, a relation between λ_A and $c'_{A_{\text{eq}}}$ is established by means of Eq. (33). Finally, in the linear viscoelastic regime the model reduces to a two-mode Maxwell model and the amplitude of the second mode is governed by the product:

$$\lambda_B n_B^0 = \text{constant},$$

where the constant is found by fitting to experiments and this then determines a relation between n_B^0 and λ_B.

Consequently, there are only three parameters to be determined for a given micellar mixture. One of these is the non-linear parameter ξ, which only appears in non-linear flows, and which determines the magnitude of the contribution from the stress/strain rate-dependent term to the overall breaking rate of the long micelles. The other two parameters to be fitted can be chosen arbitrary from the remaining five. In this study we have chosen these two parameters to be n_B^0 and $c'_{A_{\text{eq}}}$.

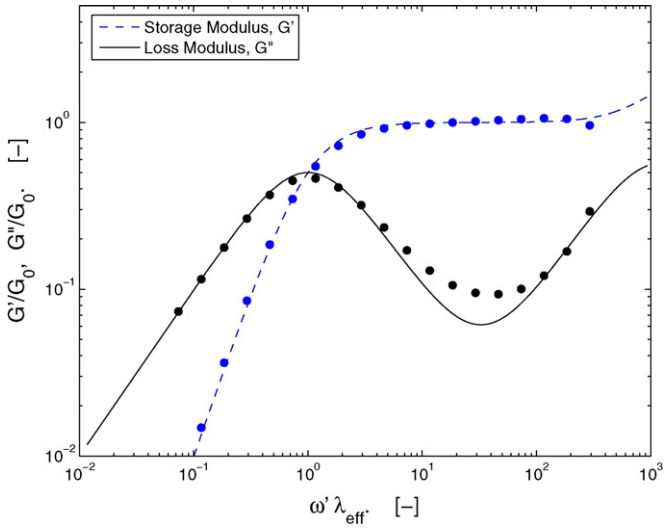

Fig. 3. Non-dimensional storage and loss modulus model prediction compared with experimental data from a solution of 100 mM CpyCl [9]. In this figure $\lambda_B n_B^0 = 1 \times 10^{-3}$ s, $\lambda_{\text{eff}} = 1.17$ s, and $G_0 = 27$Pa.

From Eqs. (32c) and (32d) the storage and loss moduli are given, in dimensional form, by

$$G' = G_0 \left\{ \frac{(\lambda_{\text{eff}}\omega')^2}{1 + (\lambda_{\text{eff}}\omega')^2} + n_B^0 \frac{(\lambda_B\omega')^2}{1 + (\lambda_B\omega')^2} \right\}, \tag{34a}$$

$$G'' = G_0 \left\{ \frac{\lambda_{\text{eff}}\omega'}{1 + (\lambda_{\text{eff}}\omega')^2} + n_B^0 \frac{\lambda_B\omega'}{1 + (\lambda_B\omega')^2} \right\} + \eta_s\omega'. \tag{34b}$$

The upturn in the dynamic moduli observed experimentally at high frequencies arises from the shorter chains, species B. The contribution to the loss modulus, G'', from the solvent viscosity is negligibly small, $\eta_s/\eta_0 = \beta = \text{O}(10^{-5})$.

If λ_{eff} and $\lambda_B n_B^0$ are held constant then the frequency dependence of the linear viscoelastic moduli remain unchanged as shown in Fig. 3. Regression of the model to experimental data [9] yields best fit values of G_0, λ_{eff} and $\lambda_B n_B^0$ as shown in Fig. 3. In Fig. 4(a) we show the effect of decreasing the effective relaxation time, by either increasing $c'_{A_{\text{eq}}}$ or decreasing λ_A according to

$$\frac{1}{\lambda_{\text{eff}}} = \frac{1}{\lambda_A} + c'_{A_{\text{eq}}},$$

and in Fig. 4(b), we show that if either n_B^0 or λ_B is increased, the contribution to the elastic moduli from the second mode (i.e. shorter chains) increases.

Next we examine the model predictions under three different non-linear deformations: step strain, steady-state shear flow, and steady-state uniaxial elongational flow. First we discuss some general considerations and asymptotic behavior of the model for these deformation histories. This is followed by exploration of model predictions under these prescribed deformation histories as the parameters $c'_{A_{\text{eq}}}$, n_B^0, and ξ are varied.

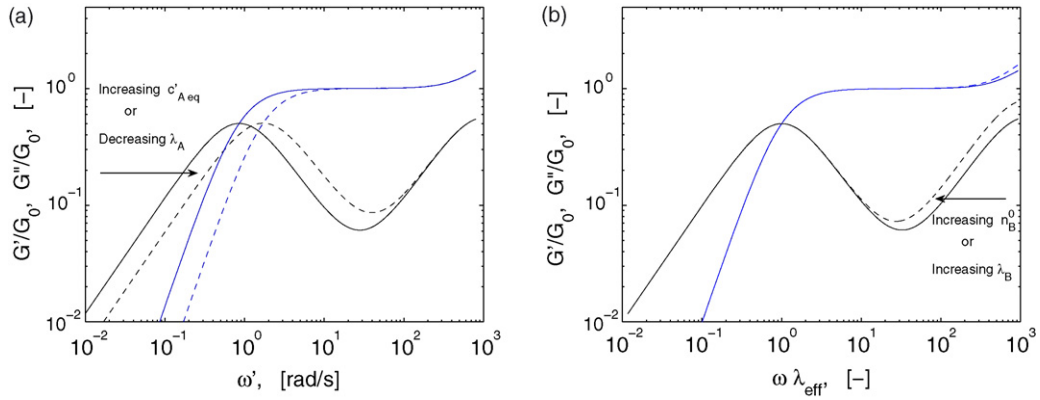

Fig. 4. Variations in the predicted loss and storage moduli: (a) effect of decreasing λ_{eff} by either increasing the breaking rate $c'_{A_{\text{eq}}}$ or decreasing the micellar relaxation time λ_A; (b) effect of increasing the number density or relaxation time of species B, n_B^0, or λ_B. Here, the solid line corresponds to the parameters in Fig. 3, the dashed line is the result arising from the variation of the indicated parameter. Other parameter values are kept as in Fig. 3.

5.1. Step strain calculations

Because the evolution equations for number density and stress are strongly coupled, it is necessary to integrate them forward in time from equilibrium conditions. To simulate actual step strain experiments, Eqs. (24)–(26), were integrated in time with an imposed strain given by

$$\gamma'(t') = \gamma'_0(1 - (1 + b't')\exp(-b't')), \tag{35}$$

where the parameter b' is obtained through fitting to the experimental motor response of a controlled strain rheometer [13]. For large b' this is the achievable experimental approximation to a Heaviside function in time. For the curves presented in this paper we have taken $b' = 127\,s^{-1}$.

Results for the stress relaxation as a function of time are shown in Fig. 5 for different applied strains. In the inset the results are graphed semi-logarithmically. It can be seen, in the inset, that for every value of γ_0 the slope of each of the parallel lines is -1, after the initial transient is completed. This indicates

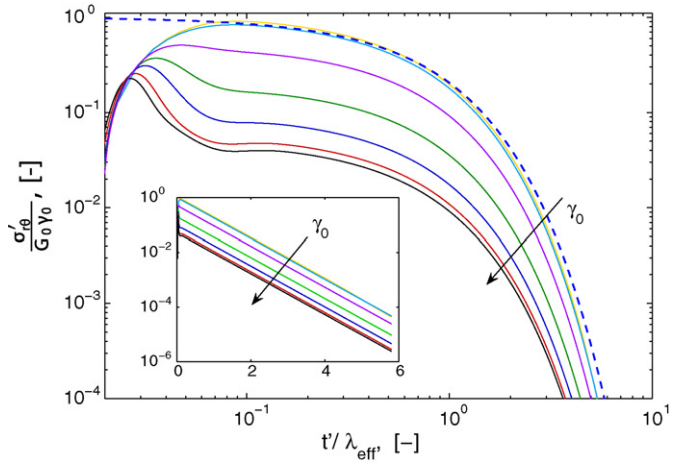

Fig. 5. Model predictions of stress relaxation after imposing a shear deformation given by Eq. (35) for $\gamma_0 = 0.1, 1, 3, 5, 7, 10, 12$. Inset: stress relaxation on linear-log scale. In this figure $\xi = 0.3$ and $\epsilon = 6.5 \times 10^{-5}$. Broken line shows the linear viscoelastic response for instantaneous shear deformation.

that the stress can be factored in the form:

$$\sigma'_{r\theta}(\gamma, t) = \gamma G_0 g(t) h(\gamma) = \gamma G(t) h(\gamma), \tag{36}$$

where the relaxation modulus is

$$G(t) = G_0 \exp(-t) = G_0 \exp\left(-\frac{t'}{\lambda_{\text{eff}}}\right) \tag{37}$$

and $h(\gamma)$ is a strain-dependent damping function. Thus, if the stress is scaled by a factor $\gamma_0 h(\gamma_0)$ all the curves will superpose. This behavior remains unchanged as long as λ_{eff} and $\lambda_B n_B^0$ are kept constant.

Analytic considerations show that the model predicts the following form of the damping function:

$$h(\gamma) = \exp\left(-\frac{\xi}{3}\gamma^2\right) + \mathrm{O}(\epsilon\mu b). \tag{38}$$

For $\varepsilon \to 0$ the relaxation is due primarily to the relaxation of species A and the damping function predicted by the model approaches,

$$h(\gamma) = \mathrm{e}^{-\xi\gamma^2/3}. \tag{39}$$

But when then terms of order $\epsilon\mu b$ are no longer negligible they have an effect on the behavior of $h(\gamma)$. The numerical best fit, for our range of values of the parameter ϵ, suggests that the damping function can be approximated by

$$h(\gamma) \approx \exp\left(-\frac{\xi}{3}\gamma^2\right) + f(\mu, b)\sqrt{\xi}\gamma \times \exp\left(-\frac{2\xi}{9}\left(\gamma - \frac{2.1}{\sqrt{\xi}}\right)^2\right). \tag{40}$$

And for the value of $b = b'\lambda_{\text{eff}}$ used in this study,

$$f \approx \frac{1}{b}\left(\frac{5}{2} - \frac{2}{\mu}\right). \tag{41}$$

Comparison of this numerical fitting with the model predictions are discussed in Section 5.4 and also presented in Fig. 7(a) below.

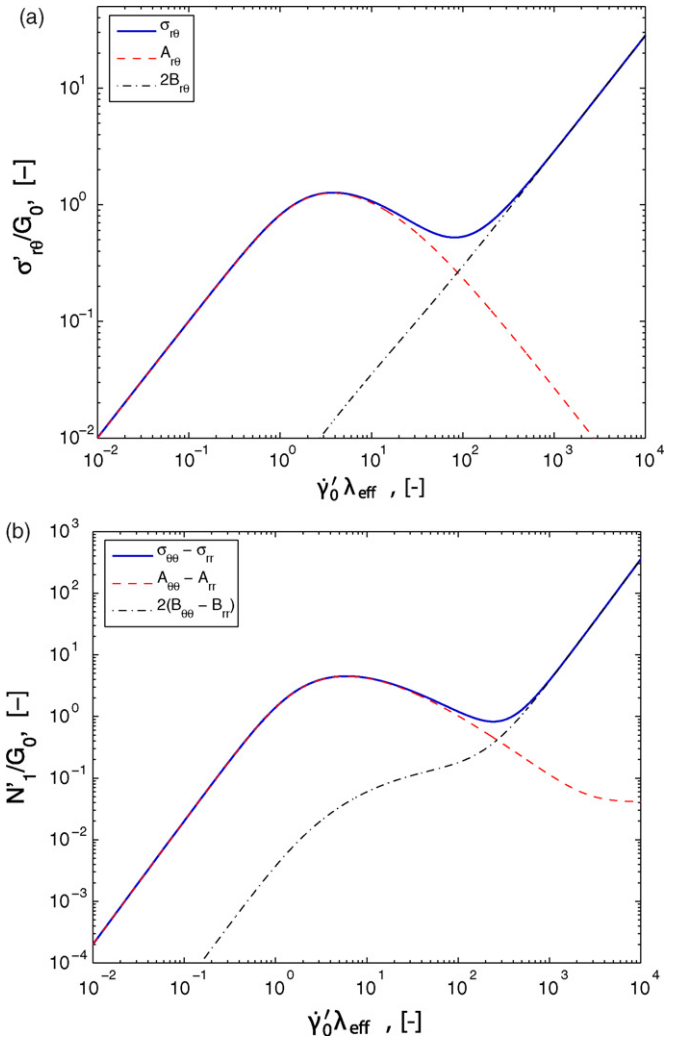

Fig. 6. Model predictions in steady-state shear flow (a) shear stress; (b) first normal stress difference, as a function of dimensionless shear rate. Here $\delta_A = \delta_B = 0$.

Note that $2.1/\sqrt{\xi} = 6.6, 3.8, 2.7$ for $\xi = 0.1, 0.3, 0.6$, respectively. This corresponds to values of the strain, γ_0, at which the Lodge–Meissner relation no longer holds, as seen in Fig. 7(b).

5.2. Homogeneous shear flow

Eqs. (24)–(26) were integrated numerically in time to steady-state subject to a constant dimensionless shear rate $\dot{\gamma}_0 = (\lambda_{\text{eff}}\dot{\gamma}'_0)$. Fig. 6 shows plots of the steady-state shear stress and the first normal stress difference as functions of shear rate. The resulting flow curves are non-monotonic. Beyond a critical deformation rate, $\dot{\gamma}_1$, the scission of the long network strands (species A) overwhelms the increased stretching that arises from increasing shear. At very high deformation rates the growth in the stress is again linear with respect to the shear rate due to the deformation of the shorter B micellar strands. Recall that

$$\sigma_{r\theta} = A_{r\theta} + 2B_{r\theta}.$$

From (24)–(26) it can be seen that for $\dot{\gamma}_0 \ll 1$, $B_{r\theta} \sim 0$ and $\sigma_{r\theta} \sim A_{r\theta} \sim \dot{\gamma}_0$.

On the other hand, at large shear rates, $\dot{\gamma}_0 \gg 1$, most of the chains of length L have been destroyed, hence the flow response is dominated by the short species which in this limit give rise to a stress of

$$B_{r\theta} \sim \left(1 + \frac{n_B^0}{2}\right)\mu\epsilon\dot{\gamma}_0,$$

so that:

$$\sigma_{r\theta} \sim 2B_{r\theta} \sim \frac{\lambda_B(2 + n_B^0)}{\lambda_{\text{eff}}}\dot{\gamma}_0.$$

The non-monotonic behavior at the intermediate rates, where contributions from both species vary due to breaking and reforming mechanisms, can be resolved only by performing inhomogeneous flow calculations in which a plateau is allowed to develop in the the stress/shear rate curve and shear bands are formed by the selection of different local shear rates and number densities. Calculations with other non-local constitutive models show that the precise shape of these curves depends on the dimensionless diffusivities, δ_A, δ_B, the flow loading history, and the geometry [21].

Additionally the model predicts, under viscometric flow conditions, that the maximum in the shear stress is given by

$$(\dot{\gamma}'_0\lambda_{\text{eff}})_{\max} = f(c_{A_{\text{eq}}}, c_{B_{\text{eq}}})\sqrt{\frac{1}{\xi}}, \tag{42a}$$

$$\left(\frac{\sigma'_{r\theta}}{G_0}\right)_{\max} = \frac{g(c_{A_{\text{eq}}}, c_{B_{\text{eq}}})}{\xi\dot{\gamma}_0} = \frac{g(c_{A_{\text{eq}}}, c_{B_{\text{eq}}})}{f(c_{A_{\text{eq}}}, c_{B_{\text{eq}}})}\sqrt{\frac{1}{\xi}}, \tag{42b}$$

where f and g are non-linear functions of the equilibrium reaction rates.

Recall that, under inhomogenous flow conditions, the curve of steady stress versus shear rate is expected to develop a plateau in solutions that exhibit shear banding. Some authors have proposed that this plateau is formed by a "top-jumping" mechanism [43], that is the value of the stress at the plateau, σ_{p}, corresponds to the maximum value of the stress, $\sigma_{\max}$, in the non-monotonic curve under homogenous flow. However, other authors have observed, theoretically and experimentally, that this is not always the case [44–47]. For our model, under inhomogenous flow conditions, the plateau is not typically realized by "top jumping" and hence the location of such a stress plateau is expected to be at a dimensionless stress value less than unity [29]. Furthermore, as pointed out by Berret et al. [48], the non-dimensional values of the shear stress and shear rate corresponding to the onset of a stress plateau in fact vary systematically with surfactant concentration. In our model, such a dependence is captured by variations in the parameters $c_{A_{\text{eq}}}$, $c_{B_{\text{eq}}}$, and n_B^0.

The predictions of the present scission/reformation model also appear to be broadly consistent with thermodynamic arguments regarding the energetics associated with the formation of a

plateau in the flow curve. If we take the scission energy reported for similar systems [49,50], $E_{\text{sciss}} \approx 4k_{\text{B}}T$, multiply it by the dimensional breaking rate, c'_A, and the number of long micelles per unit volume that have been broken at the maximum of the non-monotonic flow curve, $n'^0_A - n'_A|_{\max}$, we obtain the energy rate at which work was done per unit volume at the onset of the non-linear regime.

$$c'_A \times (n'^0_A - n'_A|_{\max}) \times E_{\text{sciss}} = 13.7\,\text{s}^{-1} \times 5.04 \times 10^{23}\,\text{m}^{-3} \times 4k_{\text{B}}T\,\text{J} \approx 276\,\text{J/m}^3\text{s}, \tag{43}$$

where $n'_A = n_A n'^0_A = n_A(G_0/k_{\text{B}}T)$ and $c'_A = c_A\lambda_A = [c_{A\text{eq}} + (1/3)\xi\mu\dot{\gamma}_0(A_{r\theta}/n_A)]/\lambda_{\text{eff}}\mu$.

We compare this value with the power dissipated per unit volume, which can be calculated from the dimensional stress and deformation rate tensor, $\boldsymbol{\sigma}' : \dot{\boldsymbol{\gamma}}'$, at the maximum of the flow curve,

$$2\sigma'_{r\theta}|_{\max} \times \dot{\gamma}'|_{\max} = 66.7\,\text{Pa} \times 3.22\,\text{s}^{-1} \approx 215\,\text{J/m}^3\text{s}. \tag{44}$$

Here the scaling parameters G_0 and λ_{eff} are taken from [9]. This estimate of the internal power dissipation is made at the maximum of the non-monotonic viscometric flow curve; the exact values at the stress plateau cannot be determined from viscometric calculations as pointed out above.

The first normal stress difference grows quadratically in the limit of small deformation rates and asymptotically approaches the limit $N_1 \to 2G'\dot{\gamma}'^2_0$ as $\dot{\gamma}'_0 \to 0$, as expected from simple fluid theory. The homogeneous solution exhibits a non-monotonicity similar to that observed in the shear stress at intermediate rates before increasing quadratically again at high rates due to the contribution of the short elastic B species. On the other hand, inspection of Eqs. (15) and (16) shows that $N_2 = \sigma_{rr} - \sigma_{zz} = 0$.

Although the precise form of the elastic first normal stress difference in the inhomogeneous shear-banding region cannot be determined without solving the full inhomogeneous equation set, we anticipate a change of slope but not a plateau in N_1. This is due to the coupling between the shear stress and the velocity field which, at least in the case of no significant changes in scission/reformation, gives rise to terms of the form $2\lambda_{\text{eff}}\sigma'_{r\theta}(\dot{\gamma}'_0)\dot{\gamma}'_0 \sim \dot{\gamma}'_0$ in the plateau region where $\sigma'_{r\theta}$ is constant.

5.3. Elongational flow

Because of the importance of micellar additives in controlling the extensional rheology of complex fluids employed in consumer applications (e.g. paints, shampoos) and in oil recovery, we also examine the predictions of the model in uniaxial elongation.

The steady extensional viscosity (in dimensionless form) is defined as,

$$\eta_{\text{E}}(\dot{\varepsilon}_0) = \frac{\sigma_{zz} - \sigma_{rr}}{\dot{\varepsilon}_0}.$$

At small elongational rates, ignoring terms of order ϵ, so that $B_{rr} = B_{\theta\theta} = B_{zz} = n^0_B/2$, and taking n^0_B and n^0_A at their equilibrium value, Eqs. (28) and (29) result in

$$\frac{4}{9}\xi^2\dot{\varepsilon}_0^4\eta_{\text{E}}^3 + \frac{2}{3}\xi\dot{\varepsilon}_0^2(2-\dot{\varepsilon}_0)\eta_{\text{E}}^2 + (1+\dot{\varepsilon}_0)(1-2\dot{\varepsilon}_0)\eta_{\text{E}} - 3 + \cdots = 0. \tag{45}$$

For linear theory, $\xi = 0$, this gives

$$\eta_{\text{E}} = 3\frac{1}{(1+\dot{\varepsilon}_0)(1-2\dot{\varepsilon}_0)} \tag{46}$$

and the long chains behave as a single convected Maxwell mode. As the dimensionless extension rate $\dot{\varepsilon}_0 = \lambda_{\text{eff}}\dot{\varepsilon}'_0 \to 0$, we have,

$$\eta_E = 3,$$

or, equivalently the Trouton ratio is $\eta'_{\text{E}}/\eta'_0 = 3$.

At large elongational rates the Larson model predicts

$$\eta'_E \simeq G_0(\tfrac{2}{3}\xi)^{-1}\dot{\varepsilon}'^{-1}_0. \tag{47}$$

Equivalently, at least for the values of μ that agree with experiments ($\mu \approx 3$), our two species model predicts

$$\eta_E \simeq f(c_{A_{\text{eq}}}, c_{B_{\text{eq}}})(\tfrac{2}{3}\xi)^{-0.95}\dot{\varepsilon}_0^{-1.5}, \tag{48}$$

where the exponent in the term containing ξ was found through numerical fitting and f is a function of the equilibrium reaction rates . For $\mu > 1$, f is given by

$$f(\mu) \simeq 2.45 + \frac{0.62}{\mu} - \frac{2.6}{\mu^2}.$$

Recall that our two species scission model would reduce to the Larson PEC model for the long species A if the number densities, n_A and n_B, were constant. Hence the difference between Eqs. (47) and (48) arises because of the additional mode of stress reduction due to the scission of the elongated chains in the two species model. Note that, from Eq. (47), Larson's one species model predicts that at large elongational rates the extensional stress difference becomes constant at a value $\eta'_{\text{E}} \approx 3G_0/2\xi$. On the other hand Eq. (48) predicts $\mu \sim 3$

$$\sigma_{zz} - \sigma_{rr} = \eta_{\text{E}}\dot{\varepsilon}_0 \sim \dot{\varepsilon}_0^{-0.5}. \tag{49}$$

The parameter μ can take on a wide range of values anywhere between 2 and 100, and the prediction is a non-monotonic stress. That is for our two species model the extensional stress reaches a maximum, $(\sigma_{zz} - \sigma_{rr})_{\max}$, at a critical elongational rate, $\dot{\varepsilon}_{\max}$. At rates greater than this maximum the extensional stress decreases. Thinning filaments of such fluids would be expected to be Hadamard unstable due to the rapid growth of high wavenumber disturbances beyond a maximum stress. Viscoelastic jets of fluids described by such a model can undergo elastic modes of rupture which do not depend on the presence or magnitude of interfacial tension [51]. Instabilities in the elongational flow of wormlike micelles have been observed in experiments [39]. Analysis of the present two species model shows that this maximum in the stress is given by

$$(\sigma_{zz} - \sigma_{rr})_{\max} = \frac{f_{\text{E}}(c_{A_{\text{eq}}}, c_{B_{\text{eq}}})}{(2\xi/3)\dot{\varepsilon}_{\max}} \tag{50}$$

where f_E is a function of the equilibrium reaction rates, and $\dot{\varepsilon}_{max}$ is the positive root of

$$a_0 + a_1\dot{\varepsilon}_{max} + (a_2 + a_3(\tfrac{2}{3}\xi))\dot{\varepsilon}^2_{max} = 0,$$

here the coefficients, a_i, are functions of the reaction rates, $c_{A_{eq}}$ and $c_{B_{eq}}$.

5.4. Model parameters

Ultimately we wish to quantitatively compare the model predictions with experimental data on the rheology of wormlike micellar solutions. We thus study the effects of varying the equilibrium breaking rate, $c'_{A_{eq}}$; the equilibrium number density of species B, n^0_B; and the parameter ξ for the three different types of deformations described above.

5.4.1. Variation of the equilibrium breaking rate

From (33) we see that once the value of λ_{eff} is set by fitting it to SAOS experiments and once a value of $c'_{A_{eq}}$ has been chosen, λ_A can be determined from the relationship:

$$\lambda_A = \frac{\lambda_{eff}}{1 - \lambda_{eff}c'_{A_{eq}}}. \tag{51}$$

Note that for λ_A to remain positive we require

$$0 \le c'_{A_{eq}} \le \frac{1}{\lambda_{eff}}.$$

In this section we consider two different limits. In the first limit $c'_{A_{eq}} \ll (1/\lambda_{eff})$, hence $\mu \sim 1$, or $\lambda_A \sim \lambda_{eff}$ since

$$\mu = 1 + c_{A_{eq}} = \frac{\lambda_A}{\lambda_{eff}}.$$

So that in this limit the effective relaxation is affected by both reptation and breaking dynamics (or in Cates' notation $\tau_{eff} \sim \tau_{breaking} \sim \tau_{reptation}$) and reptation and breaking happen on the same time scale. In the second limit, $c'_{A_{eq}} \to 1/\lambda_{eff}$ or $\mu \gg 1$ so that $\tau_{eff} \sim \tau_{breaking} \ll \tau_{reptation}$ and breakage of the chains happens more rapidly than reptation.

Fig. 7 shows predictions of the damping function for the model in step strain. It can be seen that in the regime where the breaking and reforming rates are large ($\mu \gg 1$), the damping function is softer. Asymptotic expressions for the damping function have been given earlier by Eq (39) for $\mu \sim 1$ and Eqs. (40) and (41) for the case when $\mu \gg 1$. The Lodge–Meissner relation asserts that for a step strain γ_0 the first normal stress difference N_1 is related to the shear stress σ by the relationship $N_1(t, \gamma_0) = \gamma_0\sigma(t, \gamma_0)$ [26]. In our case, with time–strain factorability, this becomes $N_1(\gamma_0) = \gamma_0 G(t)h(\gamma_0)$. Fig. 7(b) shows that for larger breaking and reforming rates the Lodge–Meissner relation is broken sooner. Interestingly the relationship is non-monotonic but always deviates below the affine relationship. Experiments suggest that the deviation from this co-linear relation, at $\gamma \sim 8$, coincides with the onset of shear banding. In a future paper [13] this phenomenon is studied, and we determine, for a given solution, which of the two limits better agrees the experimental results.

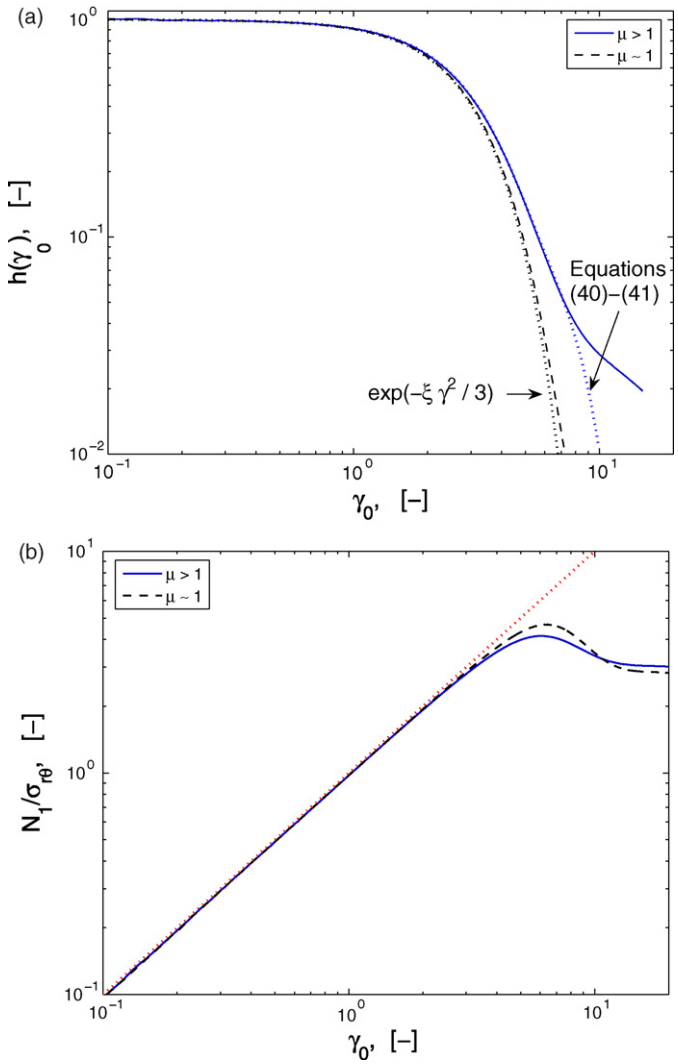

Fig. 7. Model predictions in step strain with variations in μ: (a) damping function, for $\mu \sim 1$ (broken line) the fit comes from theory and for $\mu > 1$ (solid line) the fit is numerical; (b) first normal stress difference divided by shear stress, here the dotted line demonstrates the extent of agreement with the Lodge–Meissner relation, $N_1/\sigma_{r\theta} = \gamma_0$.

Fig. 8 shows the steady shear stress and number density of the longer species as a function of shear rate for different values of the ratio $\mu = \lambda_A/\lambda_{eff}$. In the limit where $\mu > 1$, such that $c_{A_{eq}}$ and $c_{B_{eq}}$ are also large, the main relaxation mechanism in the intermediate shear-rate region is the breaking and reforming of long micelles, hence the stress is larger compared to the limit where relaxation is due to both reversible breaking and reptation. As the shear rate increases beyond $\lambda_{eff}\dot{\gamma}'_0 \sim 1$, the number density of the long species A decreases and the population balance shifts towards the shorter B chains. This gives rise (in a homogeneous analysis) to a non-monotonic flow curve. In an experiment or inhomogeneous simulation this will lead to a 'banded' flow with different number densities and orientations of the wormlike molecules in each band. Recall that the maximum in the shear stress is a function of the rates of breakage and reformation, $c_{1_{eq}}$ and $c_{2_{eq}}$, as shown in Eq. (42). Regardless of the value of μ, the stress contribution from the short species, $B_{r\theta}$, is the same for large $\dot{\gamma}_0$.

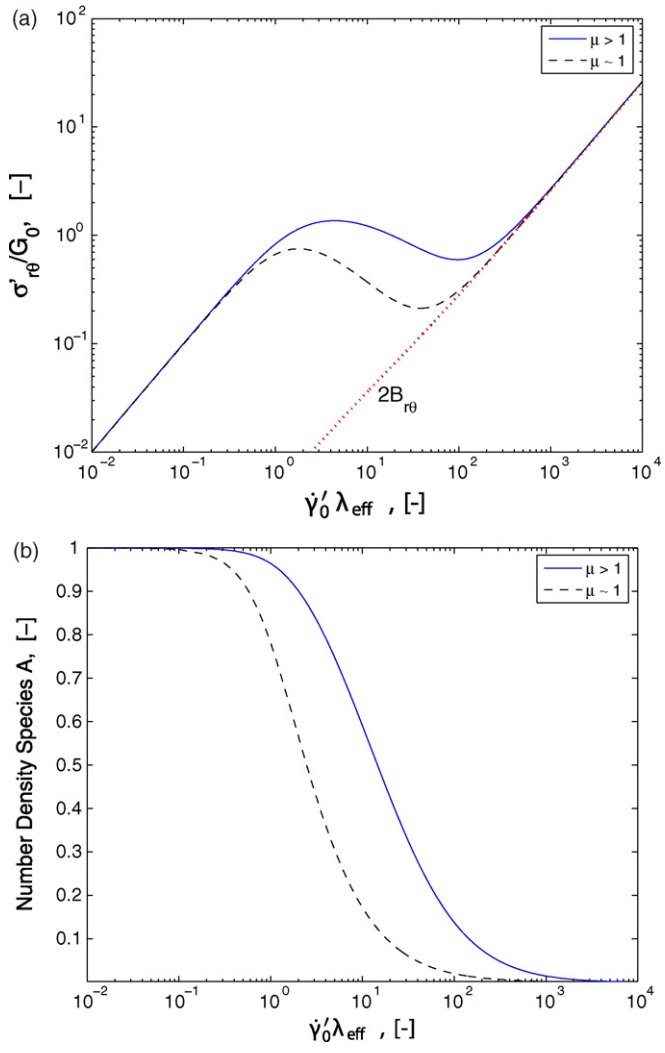

Fig. 8. Model prediction in shear flow for different values of the relaxation time ratio $\mu = \lambda_A/\lambda_{\text{eff}}$: (a) steady shear stress vs. shear rate, here the dotted line indicates the contribution to the shear stress from the short species at large shear rates and (b) number density of species A vs. shear rate. In the calculations shown by the solid line we use $\mu = 3.5$.

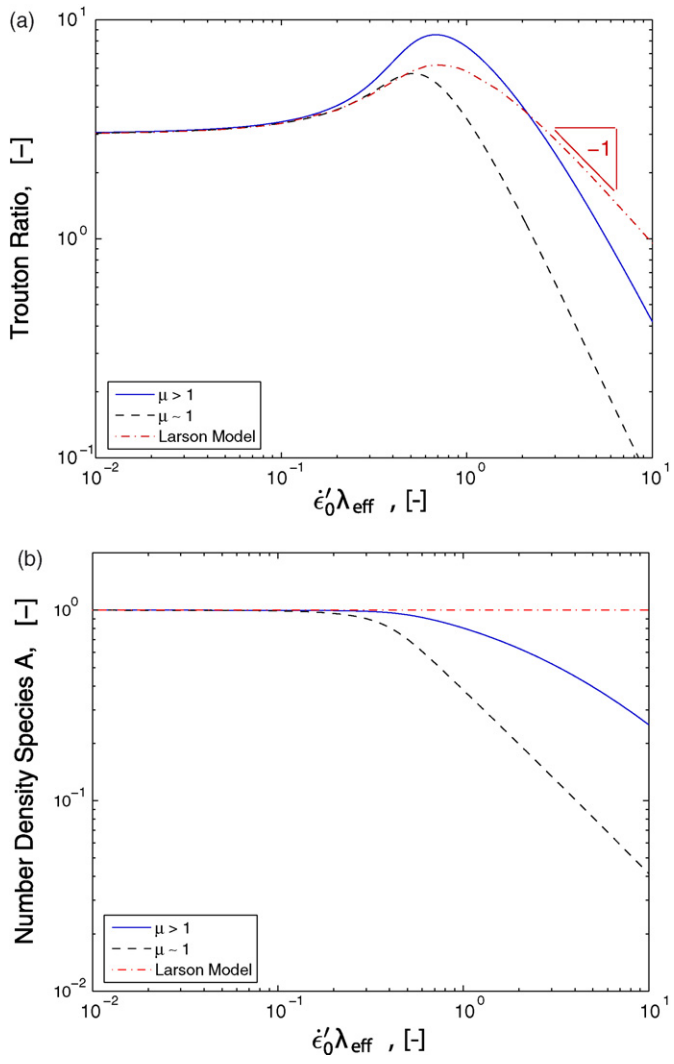

Fig. 9. Prediction of the two species model in elongational flow for different values of μ compared to predictions from the single species Larson model: (a) steady-state Trouton ratio vs. elongational rate and (b) number density of species A. The Larson model has a constant number density at all deformation rates. In this figure, $\xi = 0.3$ for all curves.

In Fig. 9, predictions of the model in steady uniaxial extensional flow for the two different limiting values of μ are compared with those of the Larson PEC model [35]. As shown in Fig. 9(a), the model first predicts an increase in the elongational viscosity due to the stretching and alignment of the micellar network segments. However, after an initial increase, the tensile stress difference saturates and the steady elongational viscosity at high rates begins to decrease. Elongational thinning is predicted by our model to be faster than that of the Larson model due to the breaking of the longer, A, species. As the breakage rate increases the number density decreases more rapidly and the extensional viscosity falls more rapidly. This decrease in the number of elongated A species at large strains reduces the total tensile stress difference further (see Eq. (49)). Beyond the point of maximum elongational viscosity, elongating micellar threads would be expected to be dynamically unstable to necking or rupture events.

5.4.2. Variations of equilibrium number density species B

In the selection of the parameter n_B^0, note that for the continuous length distribution presented in Cates' theory [14], at equilibrium the micellar length obeys an exponential distribution so that,

$$\frac{n'^0_B}{n'^0_A} = \frac{\exp((-L/2)/\bar{\ell})}{\exp(-L/\bar{\ell})}$$

or, with our non-dimensionalization (based on n'^0_A) we find,

$$n_A^0 = 1, \quad n_B^0 = \exp\left(\frac{L/2}{\bar{\ell}}\right) \tag{52}$$

where $\bar{\ell}$ is the "number average" length of the micelles. If $n_B^0 = \mathrm{e}^{\kappa}$, this corresponds to choosing the length of the short chains in the present model to be κ-times the average length as it is understood in Cates theory. Thus larger values of κ

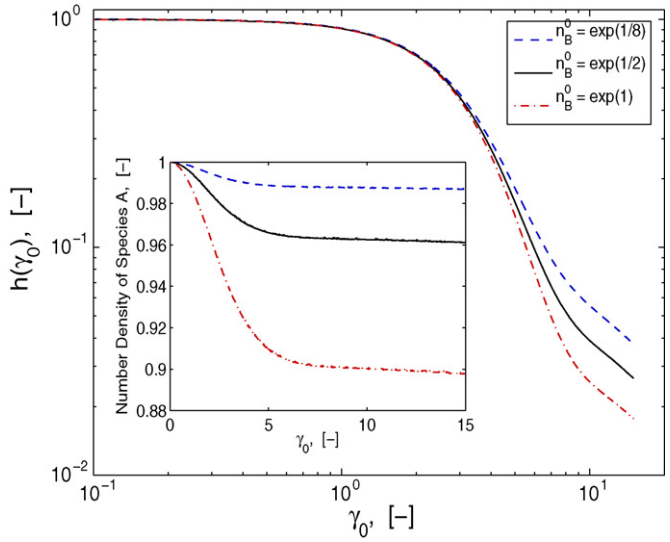

Fig. 10. Variation of the damping function vs.applied strain for different n_B^0. Inset: breaking of chains of length L as a function of the applied strain.

implies longer chains relative to $\bar{\ell}$. In this study we have chosen $\kappa = 1, 1/2, 1/8$. A value of $\kappa = 1/2$ thus corresponds to $L = \bar{\ell}$ and the long chains in our two species model are of mean length within the Cates theory. Fig. 10 shows the damping function plotted for different values of n_B^0. It can be seen that if the length of species A, at equilibrium, is longer than the average length, i.e. $\kappa > 1/2$, then after a deformation is applied species A chains will break at smaller strains than when $\kappa < 1/2$. In this section plots of the viscometric properties of shear and elongational flows are omitted since the variations, as n_B^0 changes, are qualitatively similar to that in Figs. 8 and 9. In shear flow, the maximum in the intermediate shear rate region of the curve of steady shear stress versus shear rate is higher for smaller κ because species A break less. The dependence of the maximum shear stress on the shear rate is given by Eq. (42). The curve of steady shear stress versus shear rate is unaffected in the non-monotonic regions. In extensional flow, smaller values of κ result in a larger elongational thickening.

5.4.3. *Effect of the partially extending strand parameter ξ*

Recall from Section 2.3 that the long species, A, break with a reaction rate

$$c_A = \frac{1}{3}\xi\mu\left(\dot{\boldsymbol{\gamma}} : \frac{\mathbf{A}}{n_A}\right) + c_{A_{\text{eq}}}.$$

Hence variations of the parameter ξ directly affect the breaking rate, in non-linear flows, as a function of the strain, shear rate, and elongational rate. As a consequence, smaller values of ξ result in a softer damping function, a larger steady-state shear stress, and greater elongational thickening, as seen in Figs. 11 and 12.

The value of the parameter ξ necessary to predict experimental responses of a given solution can be determined by fitting to step strain experiments, since this parameter directly affects the rate of strain softening.

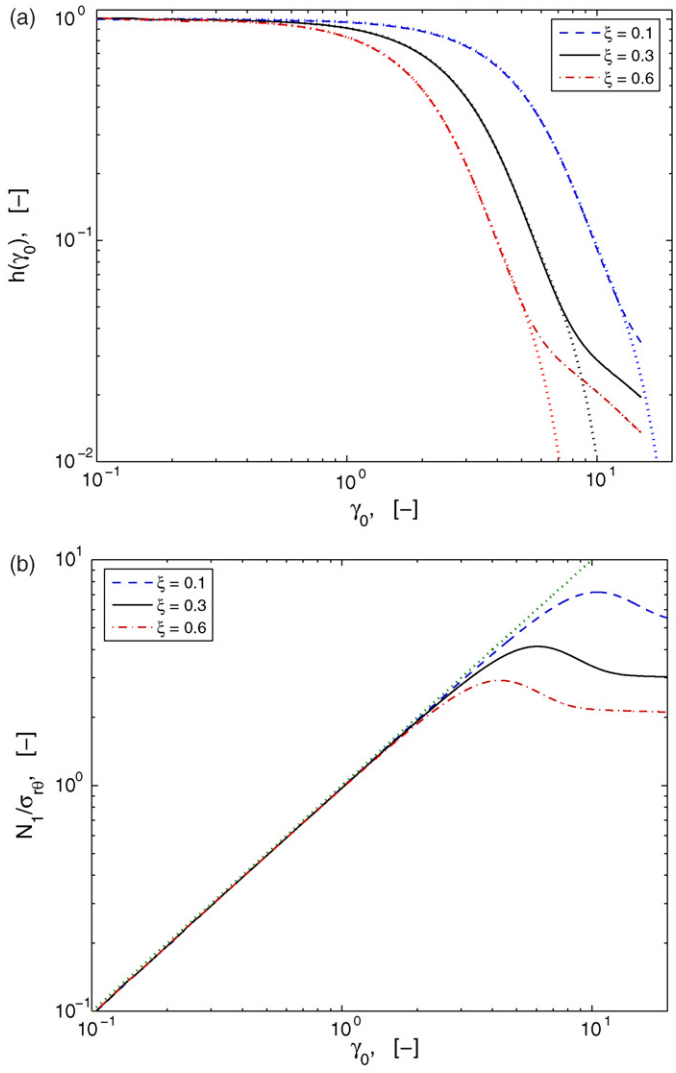

Fig. 11. Model prediction in step strain for different values of ξ:(a) damping function vs. applied strain and (b) Lodge–Meissner relation.

In Fig. 11(a), the damping function predicted by our model for different values of ξ are compared to the asymptotic expressions obtained from Eq. (40). Predictions for strains larger than 8 are studied in a future paper [29], since the onset of shear banding has been observed for strains of this order [13]. In Fig. 11(b), it is shown that the model output agrees with the Lodge–Meissner relation up to a strain value dependent on the value of the parameter ξ, with agreement up to higher values of γ for smaller ξ as anticipated.

In Fig. 12(a) the variation of the shear stress with ξ as a function of the shear rate, and in Fig. 12(b) the variation of the Trouton ratio with extension rate, are shown. As anticipated, the shear stress approaches a monotone (upper convected Maxwell like) dependence on the shear rate as ξ goes to zero, and the Trouton ratio approaches an unbounded curve at finite extension rates (again Maxwell like) as ξ goes to zero. Once regularized by ξ the Trouton ratio shows a local maximum (see Eq. (50)) followed by an extensional thinning that scales as $\dot{\epsilon}_0^{-1.5}$.

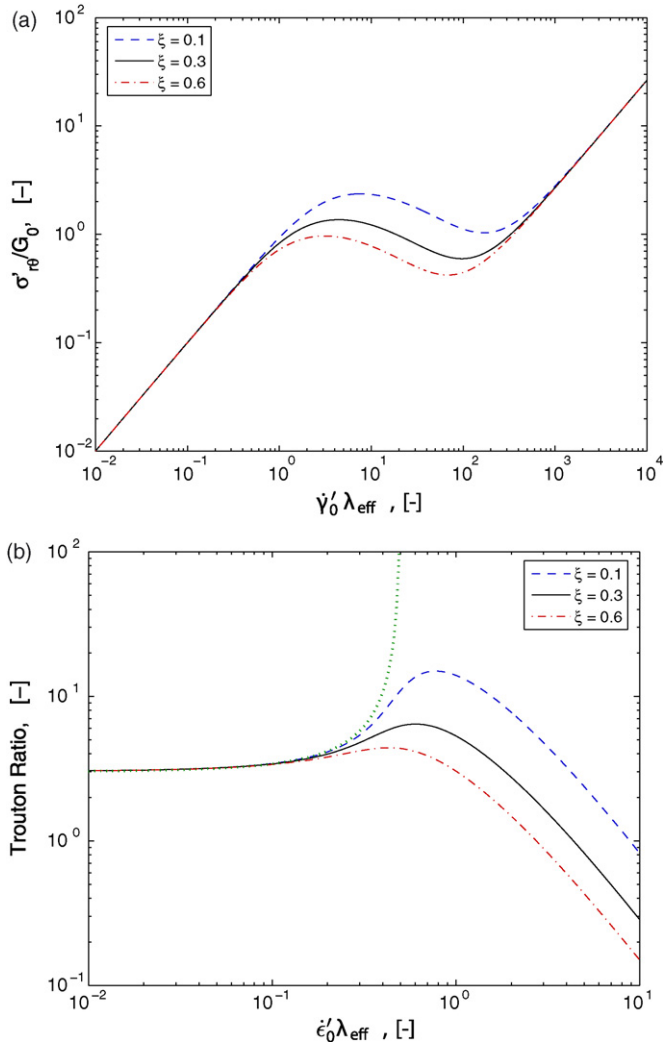

Fig. 12. Model predictions in shear and elongational flow for different values of the parameter ξ: (a) steady-state shear stress vs. shear rate and (b) steady-state Trouton ratio vs. elongational rate. In this figure the dotted line shows the asymptotic linear behavior when $\xi = 0$.

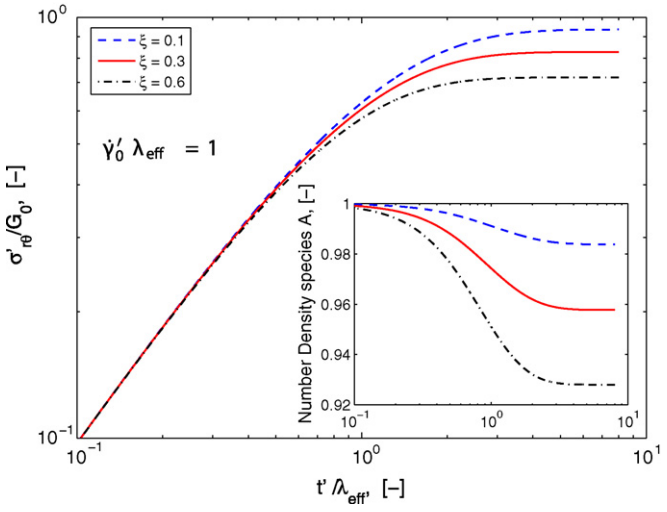

Fig. 13. Model predictions in transient shear flow for different values of the parameter ξ. Inset: variation of the number density of species A in time. Here, $\lambda_{\text{eff}} = 1.17$ s and $G_0 = 27$ Pa.

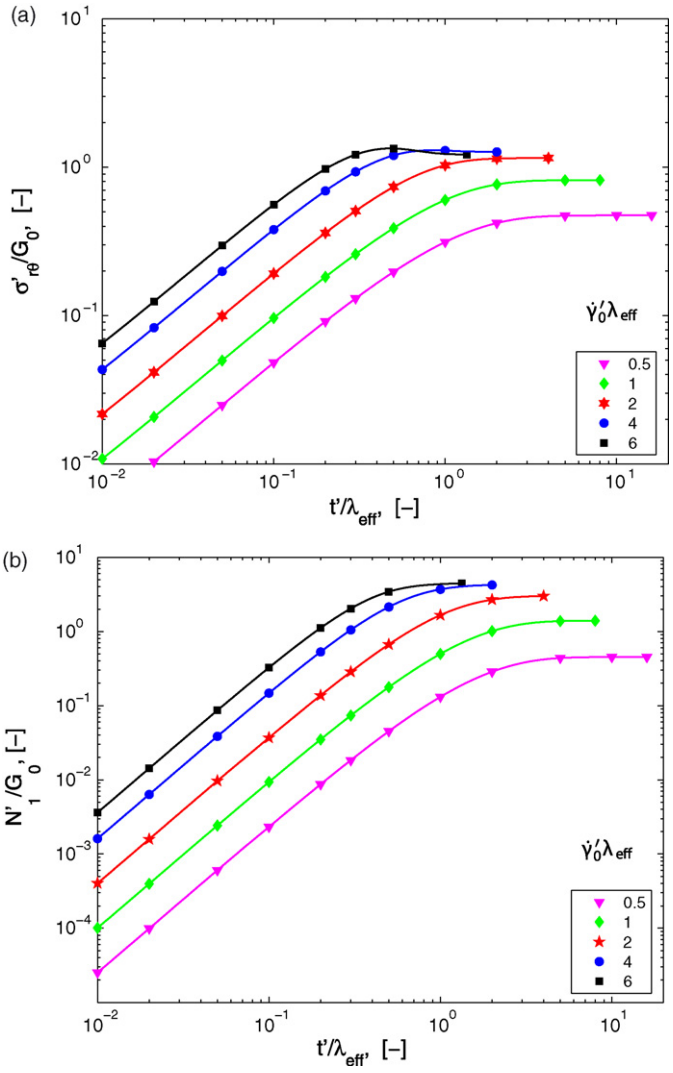

Fig. 14. Transient model predictions in homogeneous shear flow for different shear rates. Here, $\lambda_{\text{eff}} = 1.17$ s and $G_0 = 27$ Pa. (a) Shear stress vs. time and (b) first normal stress difference vs. time. Note that $\dot{\gamma}'_0\lambda_{\text{eff}} > 6$ corresponds to the non-monotonic part of the flow curve and hence shear banding is expected at these shear rates.

6. Transient response

As we have discussed above, predictions from this new constitutive model for homogenous flows are only valid in regions where the spatial variation of the number densities of the species are not important, that is regions which have not been subject to shear banding. Step strain experiments with a 100 mM CpyCl solution have shown that, for this solution, shear banding begins at a strain of $\gamma_0 \sim 8$ [13], hence constitutive predictions that assume homogenous flow are only valid up to strains of this order. Fig. 13 shows the model predictions in transient shear flow for variations of the parameter ξ at a constant shear rate $\dot{\gamma}_0 = \dot{\gamma}'_0\lambda_{\text{eff}} = 1$, the inset shows the variations of the number density of species A. Fig. 14 shows the transient predictions of the model for different shear rates. In each figure the stresses are plotted up to maximum strains of $\dot{\gamma}'_0 t' = 8$. Continuation of such curves to steady-state (corresponding to experimental

results for start up of steady shear) needs to be performed after spatial effects are re-incorporated into the equations.

7. Conclusion

We have presented a model for wormlike micellar solutions involving scission and reforming of chains based on non-affine network theory and a discrete version of Cates theory. Specifically, we consider two elastically active species, the long chains are convected by the flow and undergo rupture at a rate that depends on the deformation rate and on the local elongation rate. Following rupture the new, shorter, elastic chains partially retract before being reconnected to the network. This partially extended and convected (PEC) response is captured by a single non-linear model parameter ξ which controls the level of extension thickening in elongation and the extent of strain softening in step strain displacements. To date we have only considered Hookean elastic segments, however it is straightforward to consider numerically the role of non-linear (FENE) springs [20]. We anticipate that this will result in strain-hardening at intermediate shear strains, as observed by Brown et al. [12], and a further enhancement in the extension thickening expected in uniaxial elongation. The model, which allows for inhomogeneities in the flow kinematics, was examined in various homogenous flow situations, steady-state in a circular Couette device, step strain, steady uniaxial extension, and linear small amplitude oscillatory flow (SAOS). In each case we have explored the rheological consequences of varying the model parameters. In future papers the model predictions will be compared directly with experiments [13] and the full inhomogeneous flow field will also be explored [29].

Acknowledgments

The authors thank N.J. Kim, C. Pipe, J. Rothstein, E. Miller and L. Zhou for many helpful discussions. This work was supported by grant NSF-DMS #0405931.

References

[1] M.E. Cates, S.J. Candau, Statics and dynamics of worm-like surfactant micelles, J. Phys.: Condens. Matter 2 (1990) 6869–6892.
[2] P. Olmsted, Dynamics and flow-induced phase separation in polymeric fluids, Curr. Opin. Colloid Interf. Sci. 4 (2) (1999) 95–100.
[3] H. Rehage, H. Hoffmann, Viscoelastic surfactant solutions: model systems for rheological research, Mol. Phys. 74 (1991) 933–973.
[4] M.S. Turner, M.E. Cates, Linear viscoelasticity of wormlike micelles—a comparison of micellar reaction-kinetics, J. Phys. II France 2 (1992) 503–519.
[5] M.E. Cates, Flow behavior of entangles surfactant micelles, J. Phys.: Condens. Matter 8 (1996) 9167–9176.
[6] M.E. Cates, Nonlinear viscoelasticity of wormlike micelles (and other reversibly breakable polymers), J. Phys. Chem. 94 (1990) 371–375.
[7] G. Porte, J-F. Berret, J.L. Harden, Inhomogeneous flows of complex fluids: mechanical instability versus non-equilibrium phase transition, J. Phys. II France 7 (1997) 459–472.
[8] Y.T. Hu, A. Lips, Kinetics and mechanism of shear banding in entangled micellar solutions, J. Rheol. 49 (5) (2005) 1027–1101.
[9] E. Miller, J.P. Rothstein, Transient evolution of shear banding in wormlike micelle solutions, J. Non-Newtonian Fluid Mech. 143 (5) (2007) 22–37.
[10] J.B. Salmon, A. Colin, S. Manneville, F. Molino, Velocity profiles in shear-banding wormlike micelles, Phys. Rev. Lett. 90 (2003), 228303-1–228303-4.
[11] R.K. Prud'homme, G.G. Warr, Elongational flow of solutions of rodlike micelles, Langmuir 10 (1994) 3419–3426.
[12] E.F. Brown, W.R. Burghardt, D.C. Venerus, Tests of the Lodge–Meissner relation in anomalous nonlinear step strain of an entangled wormlike micelle solution, Langmuir 13 (1997) 3902–3904.
[13] C.J. Pipe, N.J. Kim, G.H. McKinley, P.A. Vasquez, L.P. Cook, Wormlike micellar solutions. II. Comparison between experimental data and scission model predictions, in preparation.
[14] M.E. Cates, Reptation of living polymers: dynamics of entangled polymers in the presence of reversible chain-scission reactions, Macromolecules 20 (1987) 2289–2296.
[15] J.F. Palierne, Sticky dumbbells: from Hookean dumbbells to transient network, Rheol. Acta 36 (1997) 534–543.
[16] J.G. Hernandez-Cifre, Th.M.A.M. Barenburg, J.D. Schieber, B.H.A.A. van den Brule, Brownian dynamics simulation of reversible polymer networks under shear using a non-interacting dumbbell model, J. Non-Newtonian Fluid Mech. 113 (2003) 73–96.
[17] F. Bautista, J.F.A. Soltero, J.H. Perez-Lopez, J.E. Puig, O. Manero, On the shear banding flow of elongated micellar solutions, J. Non-Newtonian Fluid Mech. 94 (2000) 57–66.
[18] M.E. Cates, Stress relaxation and chemical kinetics in pairwise associating polymers, Macromolecules 21 (1988) 256–259.
[19] B.H.A.A. van den Brule, P.J. Hoogerbrugge, Brownian dynamics simulation of reversible polymeric networks, J. Non-Newtonian Fluid Mech. 60 (1995) 303–334.
[20] A. Tripathi, K.C. Tam, G.H. McKinley, Rheology and dynamics of associative polymers in shear and extension: theory and experiments, Macromolecules 39 (2006) 1981–1999.
[21] P.D. Olmsted, O. Radulescu, C.Y.D. Lu, Johnson–Segalman model with a diffusion term in cylindrical Couette flow, J. Rheol. 44 (2) (2000) 257–275.
[22] C.Y.D. Lu, P.D. Olmsted, R.C. Ball, Effects of nonlocal stress on the determination of shear banding flow., Phys. Rev. Lett. 84 (2000) 642–645.
[23] O. Radulescu, P.D. Olmsted, Matched asymptotic solutions for the steady banded flow of the diffusive Johnson–Segalman model in various geometries, J. Non-Newtonian Fluid Mech. 91 (2000) 143–164.
[24] L.P. Cook, L.F. Rossi, Slippage and migration in models of dilute wormlike micellar solutions and polymeric fluids, J. Non-Newtonian Fluid Mech. 116 (2004) 347–369.
[25] L.F. Rossi, G.H. McKinley, L.P. Cook, Slippage and migration in Taylor–Couette flow of a model for dilute wormlike micellar solutions, J. Non-Newtonian Fluid Mech. 136 (2006) 79–92.
[26] R.G. Larson, in: H. Brenner (Ed.), Constitutive Equations for Polymer Melts and Solutions. Butterworths Series in Chemical Engineering, Butterworths, Boston, 1988.
[27] R.W. Mair, P.T. Callaghan, Shear flow of wormlike micelles in pipe and cylindrical Couette geometry as studied by nuclear magnetic resonance microscopy, J. Rheol. 41 (1997) 901–924.
[28] M.W. Liberatore, F. Nettlesheim, N.J. Wagner, L. Porcar, Spatially resolved small-angle neutron scattering in the 1–2 plane: a study of shear induced phase-separating wormlike micelles. Phys. Rev. E 73 (2006) 20504-1–20504-4.
[29] L. Zhou, L.P. Cook, P.A. Vasquez, G.H. McKinley, Modeling the inhomogeneous response in steady and transient flows of wormlike micellar solutions, in preparation.
[30] P.D. Olmsted, C.Y.D. Lu, Co-existence and phase separation in sheared complex fluids, Phys. Rev. E 56 (1997) 56–59.
[31] R.B. Bird, C.F. Curtiss, R.C. Armstrong, O. Hassager, Dynamics of Polymeric Liquids: vol. 2 Kinetic Theory, 2nd ed., John Wiley and Sons, New York, 1987.
[32] A.N. Beris, V.G. Mavrantzas, On the compatibility between various macroscopic formalisms for the concentration and flow of dilute polymer solutions, J. Rheol. 38 (5) (1994) 1235–1250.
[33] A.V. Bhave, R.C. Armstrong, R.A. Brown, Kinetic theory and rheology of dilute, non-homogeneous polymer solutions, Chem. Phys. 95 (14) (1991) 2988–3000.

[34] M. Doi, S.F. Edwards, The Theory of Polymer Dynamics, Oxford University Press, 1986.
[35] R.G. Larson, A constitutive equation for polymer melts based on partially extending strand convection, J. Rheol. 28 (1984) 545–571.
[36] G. Marrucci, F. Greco, G. Ianniruberto, Integral and differential constitutive equations for entangled polymers in simple versions of CCR and force balance in entanglement, Rheol. Act. 40 (2001) 98–103.
[37] A.E. Likhtman, R.S. Graham, Simple constitutive equation for linear polymer melts derived from molecular theory: Rolie-poly equation, J. Non-Newtonian Fluid Mech. 114 (1) (2002) 1–12.
[38] S.A. Khan, R.G. Larson, Comparison of simple constitutive equations for polymer melts in shear and biaxial and uniaxial extensions, J. Rheol. 31 (1987) 207–234.
[39] A. Bhardwaj, E. Miller, J.P. Rothstein, Filament stretching and capillary breakup extensional rheometry measurements of visocelastic wormlike micelle solutions, J. Rheol., in press.
[40] A. Bhardwaj, D. Richter, M. Chellamuthu, J.P. Rothstein, The effect of preshear on the extensional rheology of wormlike micelle solutions, Rheol. Acta, in press.
[41] D. Varade, T. Joshi, V.K. Aswal, P.S. Goyal, P.A. Hassan, P. Bahadur, Effect of salt on the micelles of cetyl pyridinium chloride, Colloid Surf. A: Physicochem. Eng. Aspects 259 (2005) 95–101.
[42] P. Fischer, H. Rehage, Non-linear flow properties of viscoelastic surfactant solutions, Rheol. Acta 36 (1997) 13–27.
[43] N.A. Spenley, M.E. Cates, T.C.B. McLeish, Nonlinear rheology of wormlike micelles, Phys. Rev. Lett. 71 (1993) 939–942.
[44] N.A. Spenley, X.F. Yuan, M.E. Cates, Nonmonotonic consitutive laws and the formation of shear-banded flows, J. Phys. II France 6 (1996) 551–571.
[45] J.F. Berret, Transient rheology of wormlike micelles, Langmuir 13 (5) (1997) 2227–2234.
[46] C. Grand, J. Arrault, M.E. Cates, Slow transients and metastability in wormlike micelle rheology, J. Phys. II France 7 (1997) 1071–1086.
[47] P. Pimenta, E.E. Pashkovski, Rheology of viscoelastic mixed surfactant solutions: effect of scission on nonlinear flow and rheochaos, Langmuir 22 (2006) 3980–3987.
[48] J.F. Berret, D.C. Roux, G. Porte, Isotropic-to-nematic transition in wormlike micelles under shear, J. Phys. II France 4 (1994) 1261–1279.
[49] J.P. Rothstein, Transient extensional rheology of wormlike micelle solutions, J. Rheol. 47 (2003) 1227–1247.
[50] B.A. Schubert, The microstructure and rheology of charged, wormlike micelles, Ph.D. Thesis, University of Delaware, 2003.
[51] M. Renardy, Self-similar breakup of Non-Newtonian fluids jets, in: D.M. Binding, K. Walters (Eds.), Rheology Reviews, 2004. pp. 171–196.